All-Inorganic Halide Perovskites for Optoelectronics: Progress and Prospects

*Jia Liang, Jie Liu, and Zhong Jin**

During the past 8 years, solution-processed organic–inorganic metal halide (OMH) perovskites have become some of the most notable materials because they can exhibit high solar cell efficiency, exceeding 20%. However, due to the volatile and hygroscopic nature of the organic cations, OMH perovskites suffer from chemical instability, especially at high temperatures. Therefore, all-inorganic metal halide (IMH) perovskites ($CsBX_3$, B = Pb, Sn, Ge; X = Cl, Br, I) are rapidly emerging as promising alternatives because of their superior stabilities and comparable properties, such as strong emission, high fluorescence quantum yield and tunable bandgap covering entire visible spectrum. Highlighted by these advantages, IMH perovskites have attracted enormous attention, indicating a promising future. In this review, the recent progress on the syntheses of IMH perovskites is outlined. In addition, the research development of IMH perovskites in optoelectronic devices, such as perovskite solar cells, photodetectors, and light-emitting diodes, is introduced. Finally, the challenges facing the field of IMH perovskites are discussed and some possible solutions based on the available literature are suggested.

1. Introduction

Organic–inorganic metal halide (OMH) perovskites have drawn tremendous attention due to their unprecedented optoelectronic properties, such as large absorption coefficient, high charge carrier mobility, long electron-hole diffusion, and tunable bandgap.[1–11] OMH perovskites with the general formula of ABX_3 compose of three different species, where A is a monovalent cation (methylammonium, $CH_3NH_3^+$, MA^+; formamidinium, $CH_3(NH_2)_2^+$, FA^+), B is a tetravalent metal cation (B = Pb; Sn; Ge), and X is a halide anion (X = Cl; Br; I).[12–15] After about 8 years of development, the power conversion efficiency (PCE) of OMH perovskite solar cells (PSCs) has reached 22.1%, which is comparable to copper indium gallium diselenide (CIGS) solar cells and close to commercial monocrystalline silicon solar cells.[16–30] Moreover, the high performances of OMH perovskites have been applied for other optoelectronic devices, such as photodetectors (PDs) and light-emitting-diodes (LEDs), showing its great potential in future.[31–39]

Despite the high performances, the OMH perovskites still face a major challenge of stability issue.[40–49] Normally, OMH perovskites display very low thermal decomposition temperatures, because they contain unstable organic monovalent cations. For instance, $MAPbI_3$ decomposes rapidly within 30 min at 150 °C in air.[50] While the black perovskite phase of $FAPbI_3$ is only stable above 160 °C and it trends to form a yellow phase below the phase transition temperature.[16] In addition to the thermal decomposition pathway, other possible degradation factors should also be carefully considered, such as degradation upon contact with moisture, light-induced trap-state formation and halide segregation.[51–54] It is known that inorganic materials usually exhibit higher stability than organic materials, especially at high temperature. Therefore, replacing the organic cations with inorganic monovalent cations in the perovskite structure was put forward. In a typical ABX_3 perovskite structure, there is a very important parameter termed as tolerance factor: $t = (R_A + R_B)/[2^{1/2}(R_X + R_B)$, where R_A, R_B, and R_X are the ionic radii of the A, B, and X ions, respectively. To maintain the symmetry of perovskite structure, the value of t should range from 0.8 to 1.1, or the cubic perovskite crystalline structure will be collapsed. The Cs^+ ion can match the requirements of t and has been regarded as an alternative inorganic monovalent cation to replace MA^+. Recently, Choi and his co-workers demonstrated an improved PCE by using a stable Cs^+/MA^+ mixed perovskite, which exhibited a higher open-circuit voltage than pure $MAPbI_3$. However, the record PCE of Cs^+/MA^+ mixed perovskite was just 7.68%.[55] Furthermore, Lee et al. reported partial substitution of Cs for FA^+ in $FAPbI_3$ perovskite, which showed a PCE as high as 19%. Moreover, Cs^+/FA^+ mixed perovskite ($FA_{0.9}Cs_{0.1}PbI_3$) displayed higher stability against the light and humidity than the $FAPbI_3$ perovskite.[56] Yi et al. echoed these results by synthesizing the Cs^+/FA^+ mixed perovskite of $FA_{0.8}Cs_{0.2}PbI_{0.84}Br_{0.16}$.[57] Saliba and his co-workers proposed a $Cs^+/MA^+/FA^+$ mixed perovskite of $Cs_{0.05}(MA_{0.17}FA_{0.83})_{0.95}Pb(I_{0.83}Br_{0.17})_3$ and employed them into the PSCs, which exhibited PCEs as high as 21.1% and good stability when exposed in ambient atmosphere.[58] Although cations mixed perovskites can display

Dr. J. Liang, Prof. J. Liu, Prof. Z. Jin
Key Laboratory of Mesoscopic Chemistry of MOE,
School of Chemistry and Chemical Engineering,
Nanjing University, Nanjing, Jiangsu 210093,
China
E-mail: zhongjin@nju.edu.cn
Prof. J. Liu
Department of Chemistry, Duke University,
Durham, North Carolina 27708, USA

DOI: 10.1002/solr.201700086

comparable performance and superior stability to those of OMH perovskites, the stability is still a problem due to the existence of organic cations.

For this reason, all-inorganic metal halide (IMH) perovskites without any organic components ($CsBX_3$, B = Pb, Sn, Ge; X = Cl, Br, I) were proposed and developed rapidly in the past 2 years.[59–65] At the initial stage, the PSCs based on IMH perovskites just exhibited PCEs of ~6%.[59] Most recently, the PCEs of IMH perovskite PSCs (based on $CsPbI_3$) have exceeded 10%.[65] In early 2015, Protesescu et al. prepared $CsPbX_3$ nanocrystals using hot-injection approach.[66] Since then, the researches on the $CsPbX_3$ nanostructures have sprung up rapidly, especially the applications in LEDs.[67–72] The latest data from Zeng's group shows that the EQE of $CsPbX_3$ based LEDs has increased from 0.12% to 6.27%.[67,72] In short, the IMH perovskites have great potential in optoelectronic applications.

Following this line of thought, in this review, we will summarize the latest progress of IMH perovskites and the applications in optoelectronic devices. The synthesis approaches of IMH perovskites, including bulk crystals, thin films and nanocrystals are firstly introduced. We then review the recent progress in optoelectronic applications of IMH perovskites, including PSCs, PDs, and LEDs. Finally, the challenges and prospects for the IMH perovskites are also discussed.

2. Synthesis of IMH Perovskites

In order to study the intrinsic properties and optoelectronic applications, various strategies were developed to synthesize IMH perovskites with different morphologies, such as bulk crystals, thin films, and nanocrystals, as shown in **Figure 1**.

2.1. Synthesis of Bulk Crystals

Whether in scientific or technological levels, growing bulk crystals of IMH perovskites is very important, because bulk crystals can reflect intrinsic physical properties.[73–77] Bulk crystals of IMH perovskites were usually prepared by Bridgman growth process, in which stoichiometric amounts of precursors were melted in a quartz tube and passed through a multi-zone tube furnace.[77] Generally, the as-synthesized IMH perovskite was a large polycrystalline ingot with smooth, bubble-free and crack-free surface, as shown in Figure 1a.

Besides the traditional solid-state Bridgman growth method, several solution-growth methods were also developed to obtain high-quality bulk crystals of IMH perovskites. For example, Dirin et al. presented a simple and fast solution phase route to grow $CsPbBr_3$ bulk crystals via an inverse temperature crystallization process.[76] Specially, Nuclei were formed by heating at 90 °C in a mixed solution containing the precursors of CsBr and $PbBr_2$, followed by heating to 110 °C for several hours. It was found that $CsPbBr_3$ bulk crystals could display high sensitivity to gamma-irradiation and good resistivity. In order to make the solution-growth method simpler, Rakita et al. developed two low-temperature methods, including slow antisolvent vapor saturation and heating a solution containing retrograde soluble $CsPbBr_3$, to produce $CsPbBr_3$ bulk crystals with high quality.[75]

2.2. Preparation of Thin Films

The preparation of perovskite thin films with pinhole-free surface was required to ensure the high performance of optoelectronic devices. Generally, OMH perovskite thin films can be fabricated by solution processes or physical deposition methods. A variety of deposition techniques, including spin-coating of precursors in one- or two-step sequential methods,

Dr. Jia Liang received his B.S. degree and Ph.D. from Southeast University in 2010 and Peking University in 2015, respectively. He joined Rice University as a visiting student in 2014. He is currently an Assistant Researcher in School of Chemistry and Chemical Engineering at Nanjing University. His research mainly focuses on synthesizing nanomaterials and their applications in perovskite solar cells, water splitting cells, and tandem cells.

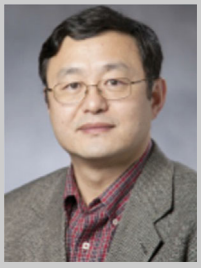

Prof. Jie Liu is currently the George B. Geller Professor of Chemistry at Duke University and an adjunct professor of "Thousands Talents" Program at Nanjing University. He earned a B.S. from Shandong University in 1987 and a Ph.D. from Harvard University in 1996. His research interests include the synthesis and chemical functionalization of nanomaterials, nanoelectronic devices, scanning probe microscopy, and carbon nanomaterials. Prof. Liu is a Fellow of the AAAS, APS, and RSC.

Prof. Zhong Jin received his B.S. (2003) and Ph.D. (2008) in chemistry from Peking University. He worked as a postdoctoral scholar at Rice University and Massachusetts Institute of Technology. Now he is a professor in School of Chemistry and Chemical Engineering at Nanjing University. He leads a research group working on functional nanomaterials and devices for energy conversion and storage.

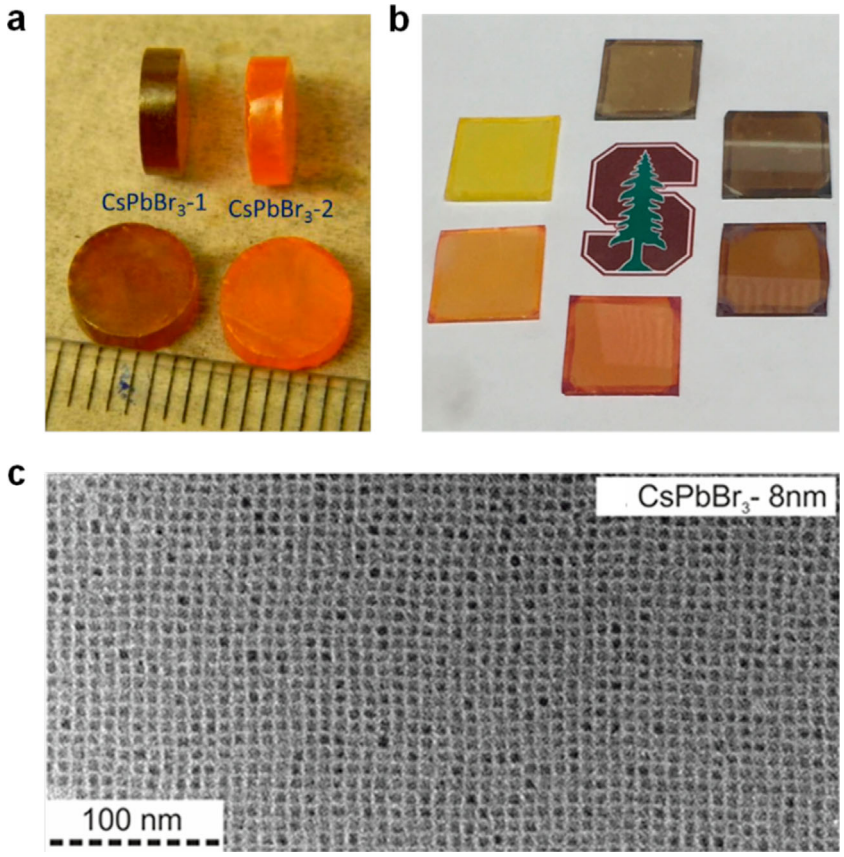

Figure 1. (a) Photograph of bulk $CsPbBr_3$.[73] Copyright 2013, American Chemical Society. (b) Photograph of $CsPbBr_3$ and $CsPb(Br_xI_{1-x})_3$ thin films.[74] Copyright 2016, American Chemical Society. (a) TEM image of $CsPbBr_3$ nanocrystals.[66] Copyright 2015, American Chemical Society.

spraying, vapor-assisted deposition, gas-assisted solution process, and dual source thermal evaporation were developed.[59,74,78,79] The one-step spin-coating method is not suitable for some IMH perovskite thin films (e.g., $CsPbBr_3$), because of the insolubility of Br-rich perovskites. While other methods for preparing OMH perovskite thin films can also be adopted to fabricate IMH perovskite thin films.[78,79] Figure 1b shows the photographs of $CsPbBr_3$ and $CsPb(Br_xI_{1-x})_3$ thin films fabricated by the two-step sequential method.[74]

IMH perovskite thin films can also be produced by spin-coating the solutions containing IMH perovskite nanocrystals.[66] However, in this method, organic capping ligands on the nanocrystals may suppress the charge transportation, leading to poor performances of corresponding devices. Thus, how to reduce the amount of long ligands for enhancing the performances of optoelectronic devices is also a hot topic, which will be discussed in the following part (section 3.3).

2.3. Synthesis of Nanocrystals

As mentioned above, colloidal IMH perovskite nanocrystals can be synthesized by various methods.[66,80–86] Right now, the mainstream method to prepare IMH perovskite nanocrystals is hot-injection approach reported by Protesescu et al. in early 2015.[66] Typically, the PbX_2 (X = Cl, Br, I) precursors were firstly dissolved in the mixed solution containing octadecene, oleylamine, and oleic acid. Then, the Cs-oleate solution was quickly injected into the mixed solution and cooled by ice-water bath. During this reaction, the nucleation and growth kinetics were very fast. After several seconds, colloidal $CsPbX_3$ nanocrystals of 4–15 nm size with cubic shape and cubic perovskite-phase crystalline structure were obtained, as shown in Figure 1c. The photoluminescence (PL) spectra of colloidal $CsPbX_3$ nanocrystals were also measured, showing narrow emission line widths of 12–42 nm, high PL quantum yield (PLQY) of 50-90%, and short radiative lifetimes of 1–29 ns. Besides these advantages, the most attractive properties of colloidal $CsPbX_3$ nanocrystals are the bandgaps, optical absorptions and emission spectra that can be tuned over the entire visible spectral region (**Figure 2**a–c). So far, two protocols were put forward to tune the bandgap and optical absorption of IMH perovskite nanocrystals.

On the one hand, changing the halide compositions of nanocrystals is an effective method to obtain IMH perovskites with different bandgaps and optical absorptions.[66,87–91] To achieve this goal, several studies have reported the synthesis of different colloidal $CsPbX_3$ nanocrystals by adding different or mixed PbX_2 salts in the process of the reaction.[66] However, due to the complicated preparation process, another method, namely anion exchange method, was introduced. The halide anions in $CsPbX_3$ nanocrystals can be easily exchanged by this method, attributing to

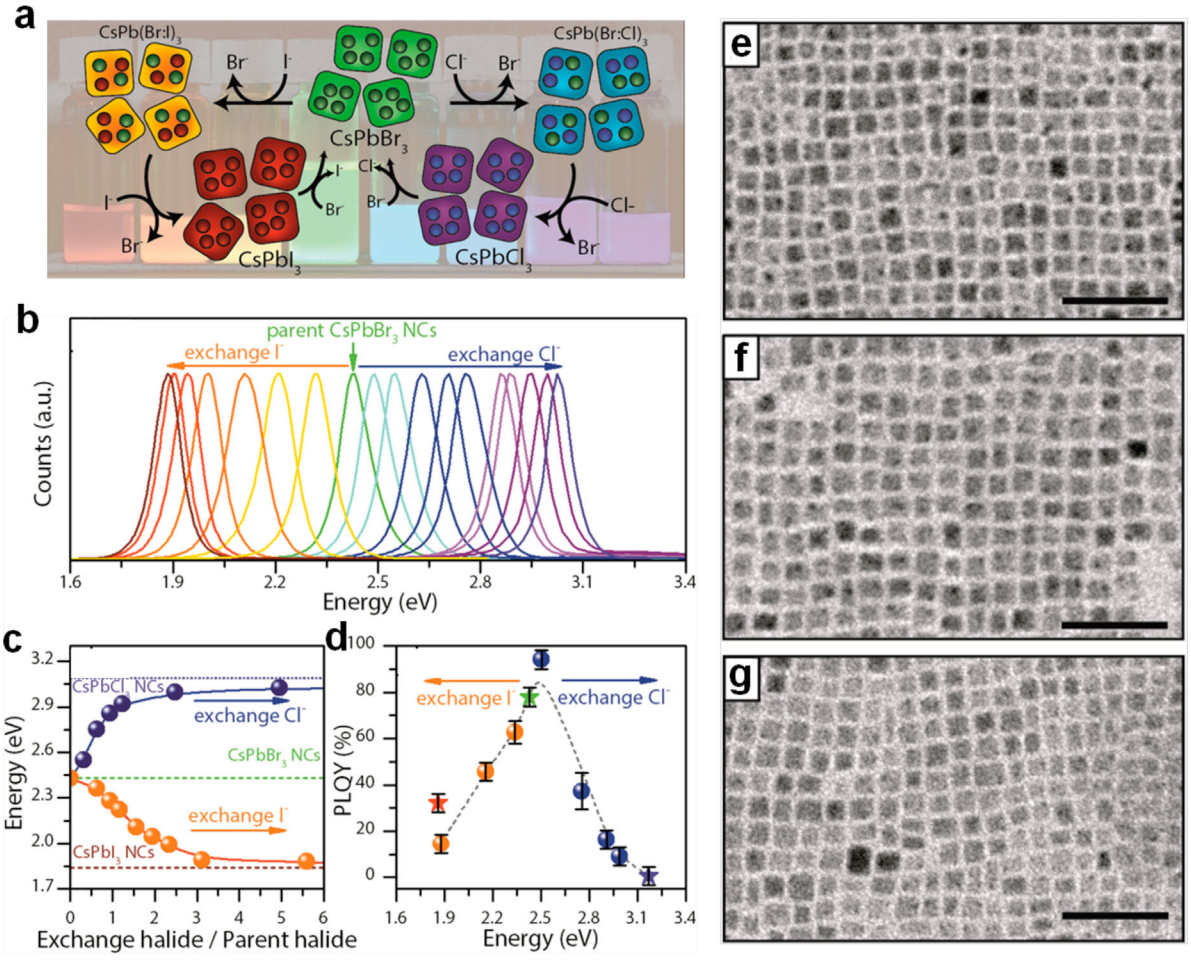

Figure 2. (a) Schematic diagram of the anion-exchange method; (b) PL spectra of $CsPb(Br:X)_3$ ($X = Cl$ or I) nanocrystals. (c) Bandgaps as a function of the exchange halides. (d) PLQY recorded on the pristine nanocrystals and halide-exchanged nanocrystals. TEM images of (e) pristine $CsPbBr_3$ nanocrystals and (f) fully exchanged $CsPbCl_3$ and (g) $CsPbI_3$ nanocrystals.[87] Copyright 2015, American Chemical Society.

the single ionic charge, the rigid nature of the cationic sublattice and an efficient vacancy-assisted diffusion mechanism.[91] Generally, the halide anion exchange could be easily achieved in the cases of Cl-to-Br, Br-to-Cl, Br-to-I, and I-to-Br. But as for the cases of Cl-to-I and I-to-Cl, it cannot be achieved because of the large difference in the ionic radii of I^- and Cl^-. Akkerman et al. demonstrated the anion exchange starting from $CsPbBr_3$ nanocrystals,[87] as a result, the PL of pristine $CsPbBr_3$ nanocrystals could be tuned within an energy range between 1.88 and 3.03 eV, as shown in Figure 2a–c. During the entire halide anion exchange process, the shape and crystal structure of the initial $CsPbBr_3$ nanocrystals were preserved (Figure 2e–g). However, the PLQYs were decreased when the Br^- ions were replaced by either Cl^- or I^- ions (Figure 2d).

On the other hand, controlling the shape and size of colloidal $CsPbX_3$ nanocrystals is another effective method to obtain different bandgaps and optical absorptions.[92–97] Some recent works reported the synthesis of colloidal $CsPbX_3$ nanocrystals with a variety of shapes (e.g., nanocubes, nanowires, nanoplates) through controlling the temperature, reaction time, and so on. Interestingly, these colloidal $CsPbX_3$ nanocrystals exhibited remarkable physicochemical, optical, and electronic properties, especially when the particle size was smaller than the Bohr radius. For example, Zhang et al.[94] prepared $CsPbX_3$ nanocubes by a modified hot-injection approach. Subsequently, they synthesized $CsPbX_3$ nanowires by controlling the reaction time (**Figure 3**a).[94] In order to decrease the diameter of $CsPbBr_3$ nanowires, they future modified the colloidal synthesis and developed a stepwise purification method (Figure 3a).[92] Because the diameter of $CsPbBr_3$ ultrathin nanowires (~2.2 nm) was below the exciton Bohr radius, large blue-shifted UV–Vis absorption and PL spectra have been observed, as shown in Figure 3b. Similar with the $CsPbX_3$ nanowires, two-dimensional (2D) $CsPbX_3$ nanoplates (Figure 3c–d) were prepared by Akkerman et al.[93] The nanoplates were grown by the injection of acetone in a mixture of precursors at room temperature. By dosing the amount of added HBr solution, the thickness of $CsPbBr_3$ nanoplates could be controlled exactly from 3 to 5 monolayers. As a result, these nanoplates displayed a narrow PL, strong excitonic absorption, and a blue shift of the bandgap due to the 2D confinement, as shown in Figure 3e.

Except for the $CsPbX_3$ nanocubes, nanowires and nanoplates, other forms of $CsPbX_3$ nanocrystals with different shapes, such

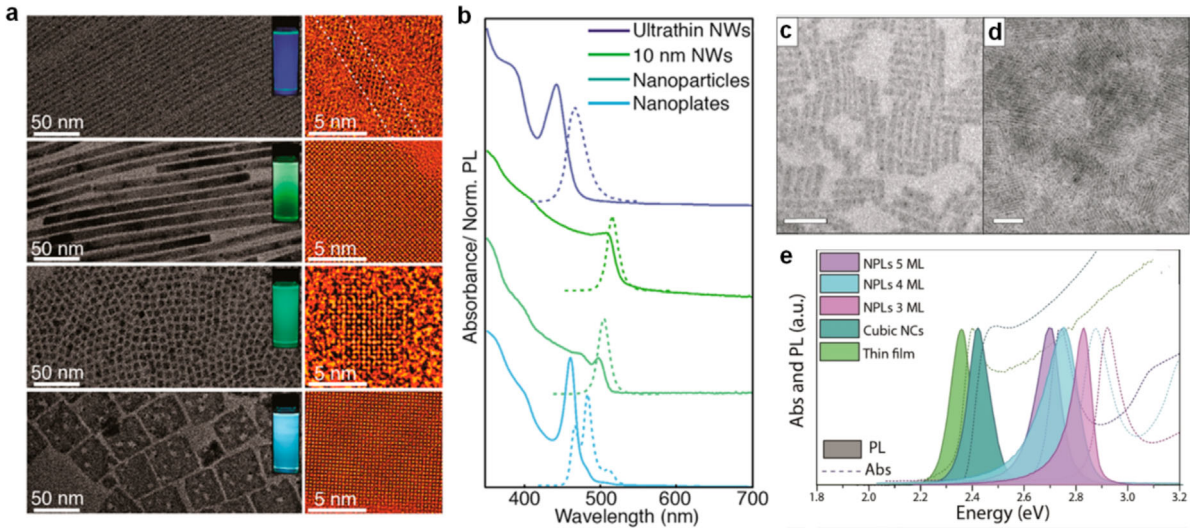

Figure 3. (a) Low-resolution TEM and aberration-corrected high-resolution TEM (AC-HRTEM) images of $CsPbBr_3$ ultrathin nanowires, 10 ± 2 nm nanowires, nanoparticles, and nanoplates. (b) Optical absorption (solid line) and PL (dash line) spectra.[92] Copyright 2016, American Chemical Society. TEM images of $CsPbBr_3$ nanoplates at (c) low concentrations and (d) high concentrations. (e) Absorption and PL spectra of $CsPbBr_3$ with the forms of thin film, cube-shaped nanocrystals, and nanoplates of different thicknesses.[93] Copyright 2016, American Chemical Society.

as quantum wires, nanorods, and so on, were also developed by other groups through altering the parameters in the growth processes.[98–101] All of them exhibited shape-dependent PL behavior and optical absorption. To clearly summarize the synthesis processes and optical properties of different $CsPbX_3$ nanocrystals, the recent developments of $CsPbX_3$ with different compositions and shapes were detailed in **Table 1**.

3. Applications of IMH Perovskites

3.1. Perovskite Solar Cells

The instability of the PSCs based on OMH perovskites has always been a serious issue. Therefore, introducing IMH perovskites into PSCs was proposed, owing to their superior

Table 1. Comparison of the photophysical properties of IMH perovskite nanocrystals with different compositions and shapes.

Materials	Shapes	Conditions	PL peaks (nm)	PLQY	References
$CsPbX_3$	Nanocubes	140–200 °C	410–700	50–90%	[66]
$CsPbBr_3$	Nanocubes	140 °C	492	79%	[82]
$CsPbBr_3$	Nanocubes	190 °C	~510	90%	[85]
$CsPbBr_3$	Nanocubes	–	520	–	[86]
$CsPbBr_3$	Nanocubes	165 °C	~520	95%	[87]
$CsPbX_3$	Nanocubes	140 °C	510–680	42–44%	[88]
$CsPbX_3$	Nanocubes	160 °C	495–513	–	[89]
$CsPbX_3$	Nanocubes	150 °C	410–700	20–80%	[91]
$CsPbBr_3$	Nanowires	160 °C	442	30%	[92]
$CsPbBr_3$	Nanoplates	150 °C	438–459	31–78%	[93]
$CsPbBr_3$	Nanowires	150–250 °C	521	–	[94]
$CsPbBr_3$	Nanoplates	150 °C	452	33%	[95]
$CsPbBr_3$	Nanoplates	130 °C	405–488	84%	[96]
$CsPbBr_3$	Nanowires	80 °C	475	–	[97]
$CsPbX_3$	Nanorods	Room temperature	505	34%	[98]
$CsPbBr_3$	Nanoplates	120–170 °C	~500	22–86%	[100]
$CsPbBr_3$	Spherical quantum dots	Room temperature	505	>80%	[101]
$CsPbX_3$	Nanorods	Room temperature	515	–	[101]
$CsPbX_3$	Nanoplates	Room temperature	510	–	[101]

stability, especially at high temperature.[59–63] Actually, the IMH perovskites have been known since the first synthesis in 1893.[102] Since then, numerous researches on their properties have been done.[103] However, most of the previous studies focused on the crystal structures or phase transitions. Recently, only a few works referred to their photovoltaic performances.[104–106] We have got much insight in the compositions, crystalline structure and phase stability of IMH perovskites from the previous literatures. The $CsPbX_3$ (X = Cl, Br, and I) perovskites can be considered as a model system of IMH perovskites. For $CsPbCl_3$ and $CsPbBr_3$, the crystal structures are tetragonally or monoclinically distorted at room temperature, and trend to convert to pure cubic perovskite structure at 47 and 130 °C, respectively.[103] For $CsPbI_3$, it is orthorhombic at room temperature and can shift to cubic perovskite structure at ~310 °C. Unfortunately, $CsPbI_3$ is unstable in cubic perovskite phase in ambient atmosphere and would rapidly convert back to the orthorhombic phase.[103] The reason for this phenomenon still remains unclear. However, because $CsPbI_3$ nanocrystals on the order of 5 nm in size are more stable than the bulk $CsPbI_3$, we consider structural stability of $CsPbX_3$ is more important than the compositional stability.[66]

Kulbak et al.[59] demonstrated that $CsPbBr_3$ was an effective absorber in the PSCs. In this report, they studied a variety of PSC architectures that have been employed in the traditional PSCs based on OMH perovskites, such as mesoporous-TiO_2 (m-TiO_2), mesoporous-Al_2O_3, and without mesoporous layer. In the three kinds of configurations, the structure of F-doped tin oxide (FTO)/compact TiO_2 layer (c-TiO_2)/m-TiO_2/$CsPbBr_3$/hole transport material (HTM)/Au exhibited the best performance (**Figure 4**a). Moreover, various HTM materials were employed in this structure, in result, poly[bis(4-phenyl)(2,4,6-trimethylphenyl) amine] (PTAA) presented the highest PCE of 5.95% with a large open-circuit voltage of 1.28 eV (Figure 4b).

To identify the stability of PSCs based on $CsPbBr_3$, Kulbak et al.[60] reported another work of direct comparison between $CsPbBr_3$ and $MAPbBr_3$ based PSCs prepared by the same method and materials except for the perovskite layer. Firstly, they compared the thermal stability of the two perovskites, confirming that the $CsPbBr_3$ can endure much higher temperature of up to 580 °C (Figure 4c). The PCE of $CsPbBr_3$ based PSCs (6.2%) was slightly lower than that of $MAPbBr_3$ based PSCs (6.5%), however, the former displayed a higher stability during the period of 2 weeks (Figure 4d–f). Finally, the two kinds of perovskites were analyzed by electron beam-induced current analysis, showing $CsPbBr_3$ was more efficient and stable under the electron beam. The results indicate that the overall performance of $CsPbBr_3$ as an absorber is over the OMH perovskite $MAPbBr_3$.

Although the two works mentioned above prepared the PSCs based on high-stability $CsPbBr_3$ films, the structures of PSCs still contained organic HTM and noble metal electrode, which were too expensive. Jin et al. proposed the design of all-inorganic PSCs, in which the organic HTMs and noble metal electrodes were completely eliminated, as shown in **Figure 5**a.[62,63] Instead, a layer of carbon electrode with a suitable work function was coated on the $CsPbBr_3$ layer. Because all the components in the PSCs are stable, the entire fabrication process can be operated in ambient environment without the need of humidity control. When this PSC was illuminated, a PCE up to 6.7% was obtained. The stability of all-inorganic PSCs was characterized, showing no performance degradation even exposed in humid air (90–95%, RH, 25 °C) without encapsulation for over 3 months. Moreover, the all-inorganic PSCs can endure both high (100 °C)

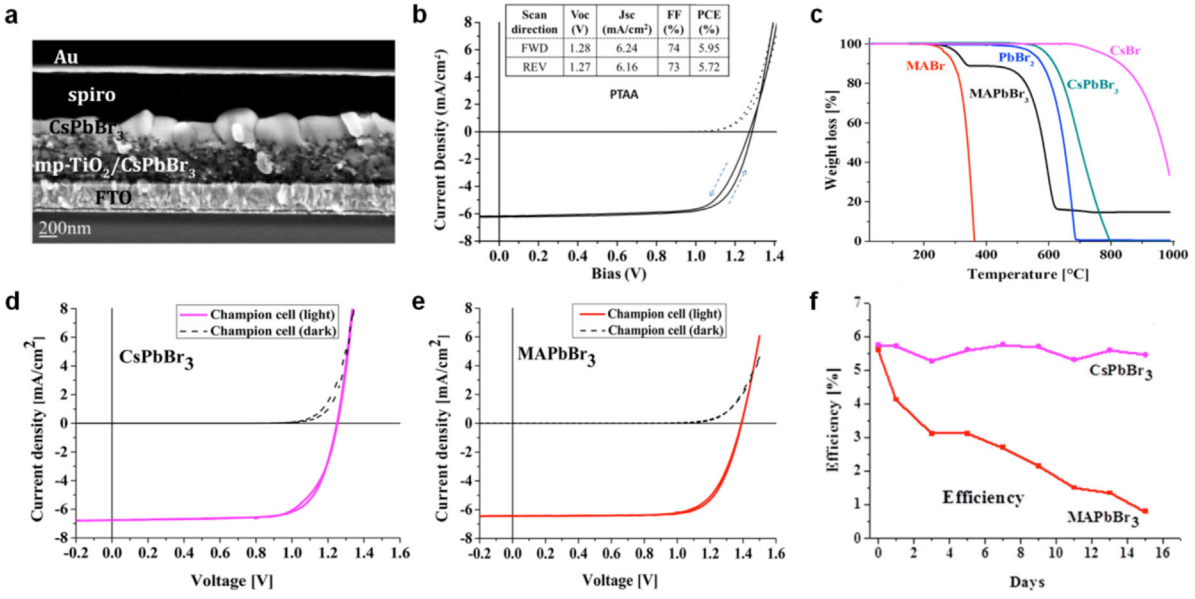

Figure 4. (a) Cross-sectional SEM image of a FTO/c-TiO_2/m-TiO_2/$CsPbBr_3$/spiro/Au solar cell. The c-TiO_2 layer on FTO glass substrate is not clearly visible in this image. (b) Light and dark J–V plots.[59] Copyright 2015, American Chemical Society. (c) Thermogravimetric analyses of MABr, $MAPbBr_3$, $PbBr_2$, $CsPbBr_3$ and CsBr. J–V plots of the best performance of the PSCs based on (d) $CsPbBr_3$ and (e) $MAPbBr_3$ in the dark and under illumination, respectively. (f) PCE of the PSCs based on $CsPbBr_3$ as a function of time.[60] Copyright 2015, American Chemical Society.

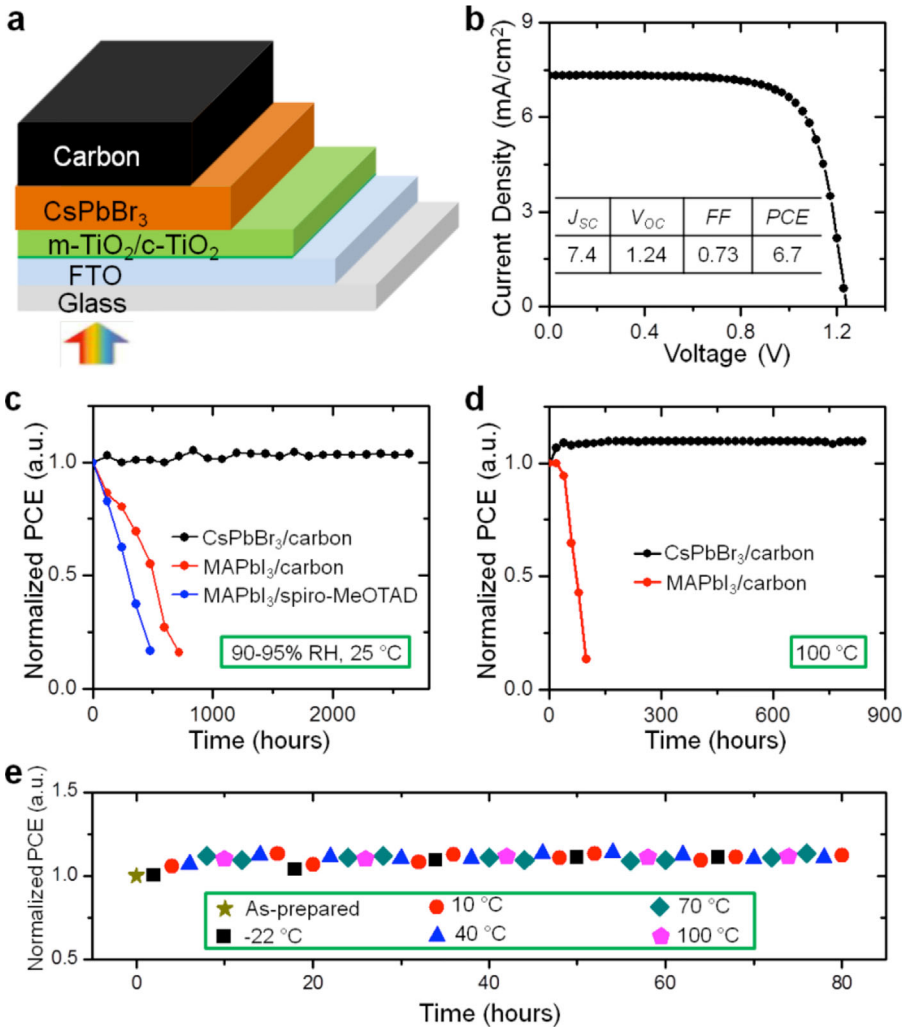

Figure 5. (a) Schematic cross-section view and (b) *J–V* plot of $CsPbBr_3$/carbon based all-inorganic PSCs. The inset in (b) shows the corresponding photovoltaic parameters. (c) Normalized PCEs of $CsPbBr_3$/carbon based all-inorganic PSCs, $MAPbI_3$/carbon and $MAPbI_3$/spiro-MeOTAD based hybrid PSCs as a function of storage time. (d) Normalized PCEs of $CsPbBr_3$/carbon based all-inorganic PSCs and $MAPbI_3$/carbon based hybrid PSCs as a function of time heated at 100 °C. (e) Normalized PCEs of $CsPbBr_3$/carbon based all-inorganic PSCs as a function of storage time during temperature circles (between −22 and 100 °C).[62,63] Copyright 2016, American Chemical Society.

and low (−22 °C) temperature, and exhibit good stability in the environment of extreme temperature cycling.

The $CsPbBr_3$ based PSCs showed excellent stability, however, in terms of the light absorption range, $CsPbBr_3$ was not an ideal absorber for PSCs due to its large bandgap (~2.3 eV). Among $CsPbCl_3$, $CsPbBr_3$ and $CsPbI_3$, the best choice should be $CsPbI_3$ with a smallest bandgap of ~1.73 eV. However, as mentioned above, $CsPbI_3$ in the black cubic perovskite phase is unstable in ambient atmosphere and will rapidly convert to yellow non-perovskite phase. Though when the size of $CsPbI_3$ particles decreased to several nanometers, the black cubic perovskite phase would be stable in the ambient atmosphere. However, the size of most of $CsPbI_3$ materials obtained from conventional methods, such as spin-coating, thermal evaporation and so on, are very large, thus having very poor stability in the ambient atmosphere.[107–109] Moreover, although $CsPbI_3$ has a suitable bandgap, the performances of $CsPbI_3$ based PSCs are not satisfying. Snaith group reported a spin-coated stable $CsPbI_3$ films by adding HI into the precursor solution and demonstrated the highest PCE of 2.9%.[107] Furthermore, Luo et al. developed a new low-temperature solution method and prepared stable $CsPbI_3$ films.[108] However, the PSCs with the structure of FTO/c-TiO_2/m-TiO_2/$CsPbI_3$/Spiro-MeOTAD/Ag exhibited a low PCE of 4.13%. Even using the inverted structure, the PCE of $CsPbI_3$ based PSCs was still not very high (5.38%).[109]

Combining the good stability of $CsPbBr_3$ and the small bandgap of $CsPbI_3$, the halide mixed perovskites of CsPb$(I_{1-x}Br_x)_3$ were proposed, such as $CsPbIBr_2$ and $CsPbI_2Br$. In order to maintain the stability of the CsPb$(I_{1-x}Br_x)_3$, $CsPbIBr_2$ was first introduced. Ma et al.[79] reported a dual source thermal evaporation process to fabricate $CsPbIBr_2$ films, showing a bandgap (2.05 eV), which was smaller than that of $CsPbBr_3$ (**Figure 6**a). Moreover, the $CsPbIBr_2$ films displayed good thermal stability in either N_2 environment or ambient

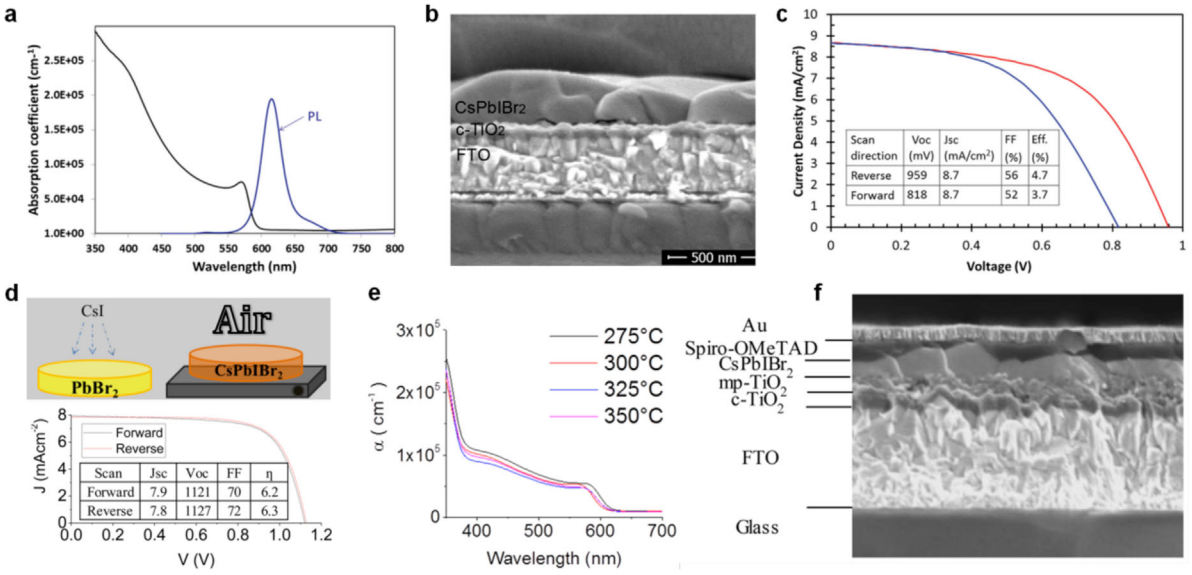

Figure 6. (a) Absorption and PL spectra of $CsPbIBr_2$ film. (b) Cross-sectional SEM image of a PSC with the structure of FTO/c-TiO_2/$CsPbIBr_2$/Au. (c) *J–V* plots of the PSC in (b).[79] Copyright 2016, Wiley-VCH. (d) Schematic diagram of the spray-assisted deposition method and *J–V* plots of the as-prepared PSC in (f). (e) Absorption spectra of the $CsPbIBr_2$ films annealed at different temperatures. (f) Cross-sectional SEM image of a PSC with the structure of FTO/c-TiO_2/m-TiO_2/$CsPbIBr_2$/Spiro-MeOTAD/Au.[110] Copyright 2016, American Chemical Society.

atmosphere. Finally, when the $CsPbIBr_2$ films were employed into the PSCs with the structure of FTO/c-TiO_2/$CsPbIBr_2$/Au, a PCE of 4.7% was obtained (Figure 6b–c). By using a spray-assisted deposition method, Lau et al.[110] also prepared $CsPbIBr_2$ films with an alike bandgap of 2.02–2.06 eV (Figure 6d–e). By adjusting the preparation conditions of $CsPbIBr_2$ films, such as the substrate temperature during spraying and the post-annealing temperature, the $CsPbIBr_2$ based PSCs displayed a stabilized PEC of 6.3% with negligible hysteresis (Figure 6d and f).

Despite $CsPbIBr_2$ exhibits smaller bandgap than $CsPbBr_3$, the PCEs of the $CsPbIBr_2$ based PSCs are not very high till now.

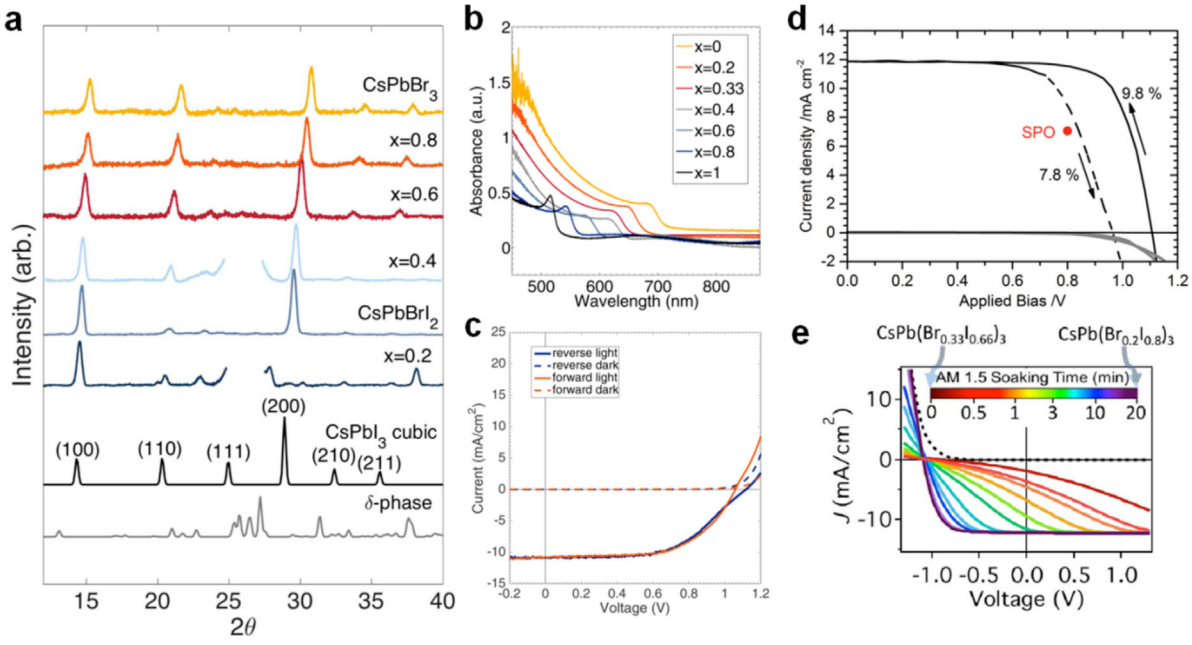

Figure 7. (a) XRD patterns and (b) absorption spectra of $CsPb(I_{1-x}Br_x)_3$ films, where $x = 0$ to 1. (c) *J–V* plot of $CsPbI_2Br$ based PSCs.[74] Copyright 2016, American Chemical Society. (d) *J–V* plots of the PSCs based on $CsPbI_2Br$ film.[78] Copyright 2016, Wiley-VCH. (e) *J–V* plots of the PSCs based on $CsPbI_2Br$ film under continuous illumination.[111] Copyright 2017, American Chemical Society.

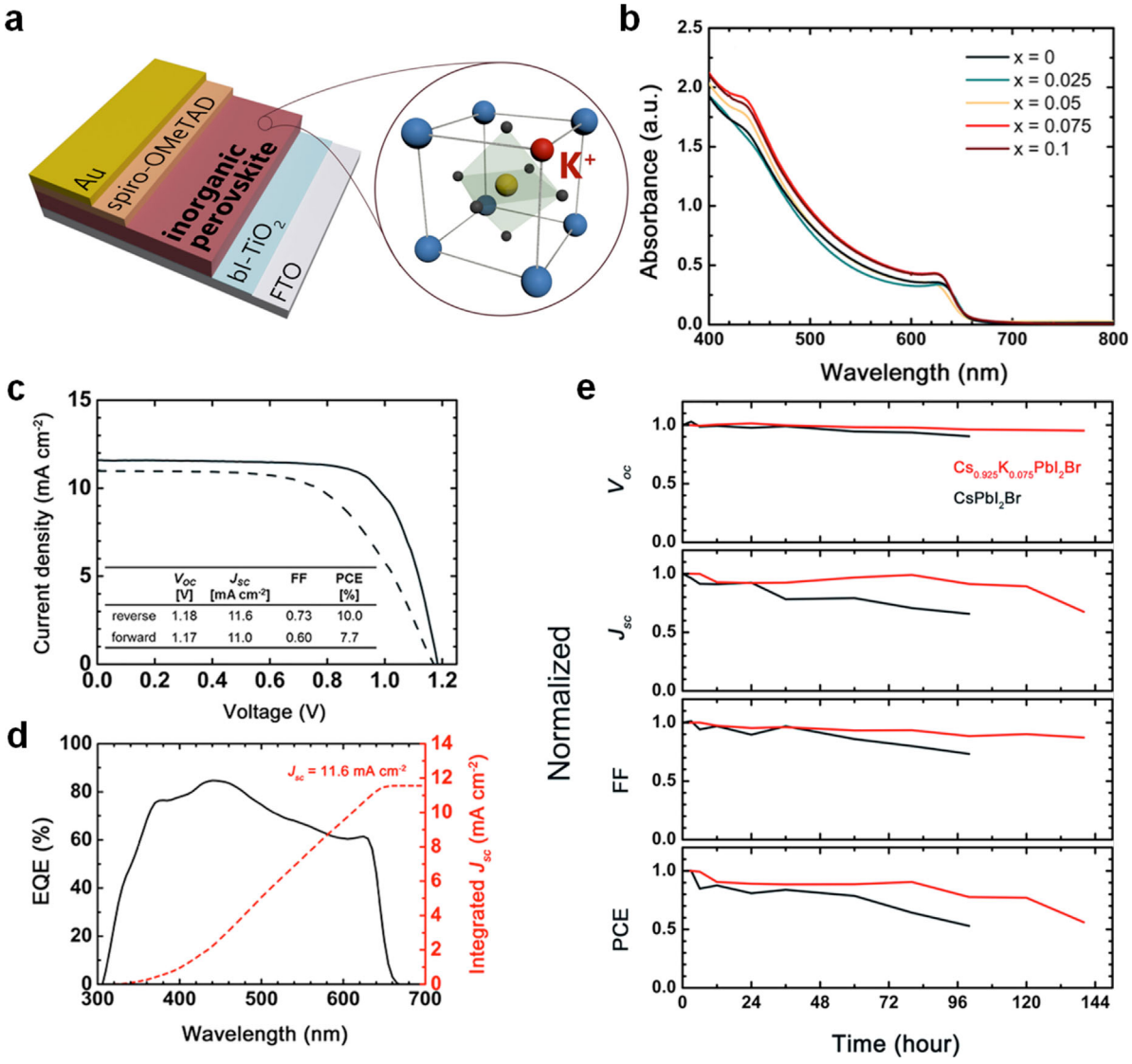

Figure 8. (a) Schematic diagram of the PSCs based on $Cs_{0.925}K_{0.075}PbI_2Br$. (b) Absorbance spectra of $Cs_{1-x}K_xPbI_2Br$ films ($x = 0$ to 0.1). (c) *J*–*V* plots and (d) IPCE spectrum of the PSCs based on $Cs_{0.925}K_{0.075}PbI_2Br$. (e) Photovoltaic parameters as a function of the time.[112] Copyright 2017, American Chemical Society.

Further reducing the bandgap of $CsPb(I_{1-x}Br_x)_3$ films by substituting Br^- with I^- is necessary. Though one-step spinning method, Beal et al. prepared $CsPbI_2Br$ films with a bandgap (1.9 eV) smaller than $CsPbBr_3$ and $CsPbIBr_2$ films,[74] and investigated the structures and absorption spectra of a series of $CsPb(I_{1-x}Br_x)_3$ films with different I/Br ratios (**Figure 7**a–b). Moreover, $CsPbI_2Br$ films exhibited good stability when it was exposed into constant illumination or high temperature conditions. The $CsPbI_2Br$ based PSCs with inverted architecture can exhibit champion and average PCEs of 6.69 and 6.5%, respectively (Figure 7c). Clearly, the PCEs were slightly higher than that of the PSCs based on $CsPbBr_3$ and $CsPbIBr_2$ films, however, the photocurrent density of 10.9 mA cm^{-2} obtained in this study is smaller than the theoretical value of 17.1 mA cm^{-2} for a 1.9 eV-bandgap material, perhaps owing to the low solubility of CsBr. Therefore, it is desirable to change the preparation method and develop a new processing route that yields thicker films with better morphology. Considering this problem, Snaith group fabricated the $CsPbI_2Br$ films by the two-step method.[78] However, it was difficult to achieve uniform films using this method. Subsequently, they also used the one-step method to prepare the PSCs based on $CsPbI_2Br$ films with the different structure from Beal et al. reported. Because of the most professional technique in their group, a champion PCE of 9.84% was obtained (Figure 7d). Intriguingly, an interesting phenomenon in the PSCs based on $CsPbI_2Br$ films was found: PSCs based on $CsPbI_2Br$ films exhibited extreme device performance evolution under continuous illumination, as shown in Figure 7e.[111] Through decoupling charge collection in the electron- and hole-transporting layers,

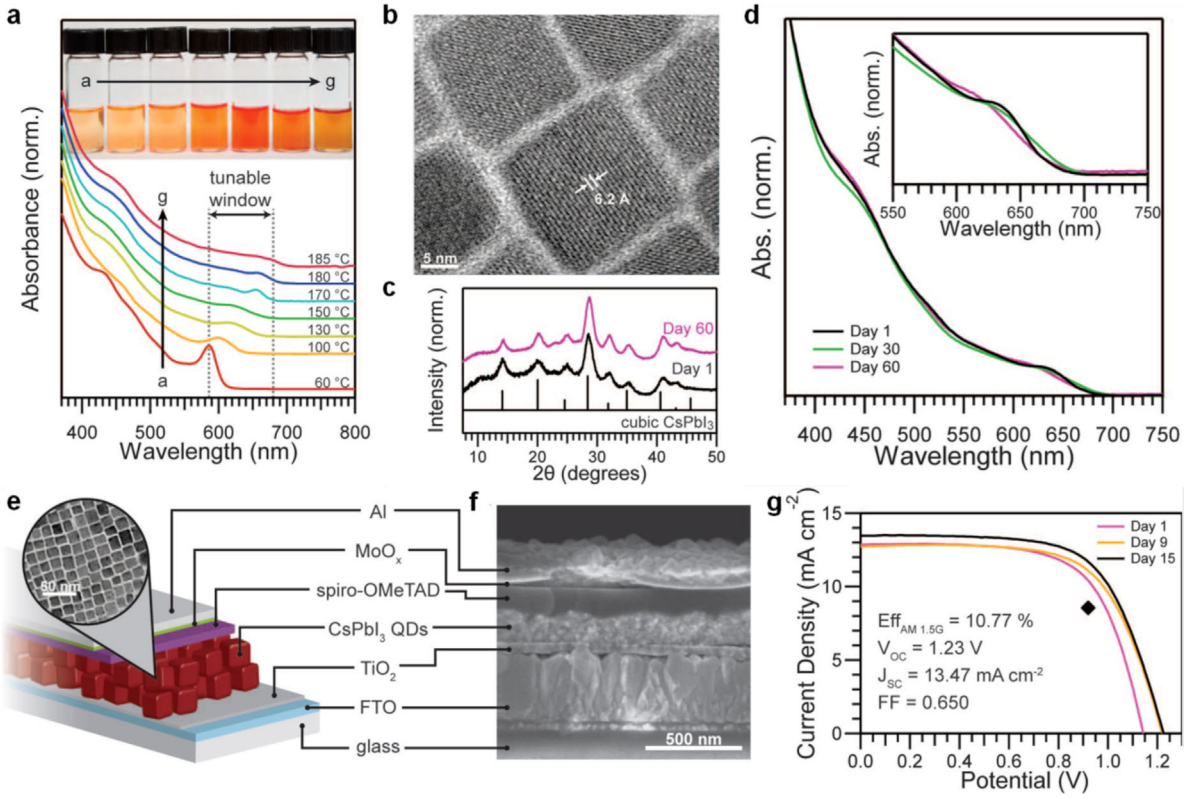

Figure 9. (a) Normalized UV–Visible absorption spectra and photographs of $CsPbI_3$ QDs synthesized at different temperatures. (b) TEM image of $CsPbI_3$ QDs. (c) XRD patterns (d) adsorption spectra of $CsPbI_3$ QDs before and after 60 days stored in ambient atmosphere. (e) Schematic and (f) cross-sectional SEM image of the PSCs based on $CsPbI_3$ QD films. (g) *J–V* plots of the PSCs based on $CsPbI_3$ QD films before and after 15 days stored in ambient atmosphere.[65] Copyright 2016, American Association for the Advancement of Science.

photoluminescence, X-ray diffraction, and solar cell device characterization, this phenomenon was mainly ascribed to the light-induced dealloying of $CsPbI_2Br$ films and thus improving the hole collection in PSCs.

Although $CsPbI_2Br$ films show good stability under constant illumination or high temperature conditions, the stability in the ambient atmosphere is still poor. In order to resolve this issue, Nam et al. incorporated potassium cations into the $CsPbI_2Br$ films (**Figure 8**a).[112] By varying the stoichiometric ratio of K^+, the properties of the $Cs_{1-x}K_xPbI_2Br$ film can be adjusted. When $x = 0.075$, the $Cs_{0.925}K_{0.075}PbI_2Br$ film showed a significant increase in absorbance intensity over the entire wavelength (Figure 8b), and exhibited the maximum and average PCEs of 10.0 and 9.1% in PSCs, respectively (Figure 8c–d). Furthermore, the PSCs based on $Cs_{0.925}K_{0.075}PbI_2Br$ films displayed higher stability that those based on $CsPbI_2Br$ (Figure 8e). The results suggest that the stability of IMH perovskites can be further improved by incorporating some specific cations into the unit cells, such as Ag^+, Bi^{3+}, and so on.

Actually, the bandgaps (1.9 eV) of $CsPbI_2Br$ films were still slightly large if they were used as the absorber materials in PSCs. Therefore, further reducing the bandgap of $CsPb(I_{1-x}Br_x)_3$ is still necessary. One of the methods was that we further substituted the Br^- ions by I^- ions, that is, the $CsPbI_3$ films. However, in the initial of this section, we have pointed out that the stability of the bulk $CsPbI_3$ was very poor. As we know, many physical properties of nanometer-sized materials may be different from bulk materials of the same chemicals. It was reported that when the size of $CsPbI_3$ nanocrystals was reduced to ~5 nm, they will become more stable than bulk $CsPbI_3$.[66] This can be ascribed to the contribution of surface energy. Swarnkar et al. developed a process to purify $CsPbI_3$ quantum dots (QDs) by using methyl acetate, an antisolvent that can isolates the $CsPbI_3$ QDs without full removal of surface species, which is critical to phase-stable photovoltaic devices.[65] Subsequently, Swarnkar et al. fabricated $CsPbI_3$ films using the stable $CsPbI_3$ QDs. They firstly spun-cast the octane solution of $CsPbI_3$ QDs, and then treated in a saturated MeOAc solution of either $Pb(OAc)_2$ or $Pb(NO_3)_2$ for several times (**Figure 9**a–b). The $CsPbI_3$ QDs films exhibited good stability when exposed into the ambient atmosphere for 60 days (Figure 9c–d). The PSCs based on $CsPbI_3$ QD films showed a PCE up to 10.77% and a large open-circuit voltage of 1.23 eV (Figure 9e–g).

Apart from the $CsPbX_3$ IMH perovskites, the lead-free IMH perovskites of $CsSnX_3$ (X = Cl, Br, I) were also investigated. In general, the bandgaps of $CsSnI_3$ and $CsSnBr_3$ are 1.27 and 1.75 eV, respectively, which are very suitable for serving as the absorbers in PSCs. However, the performances of PSCs based on $CsSnX_3$ IMH perovskites are still less than satisfactory.[115,116] One of the main reasons is the instability caused by the Sn-cation

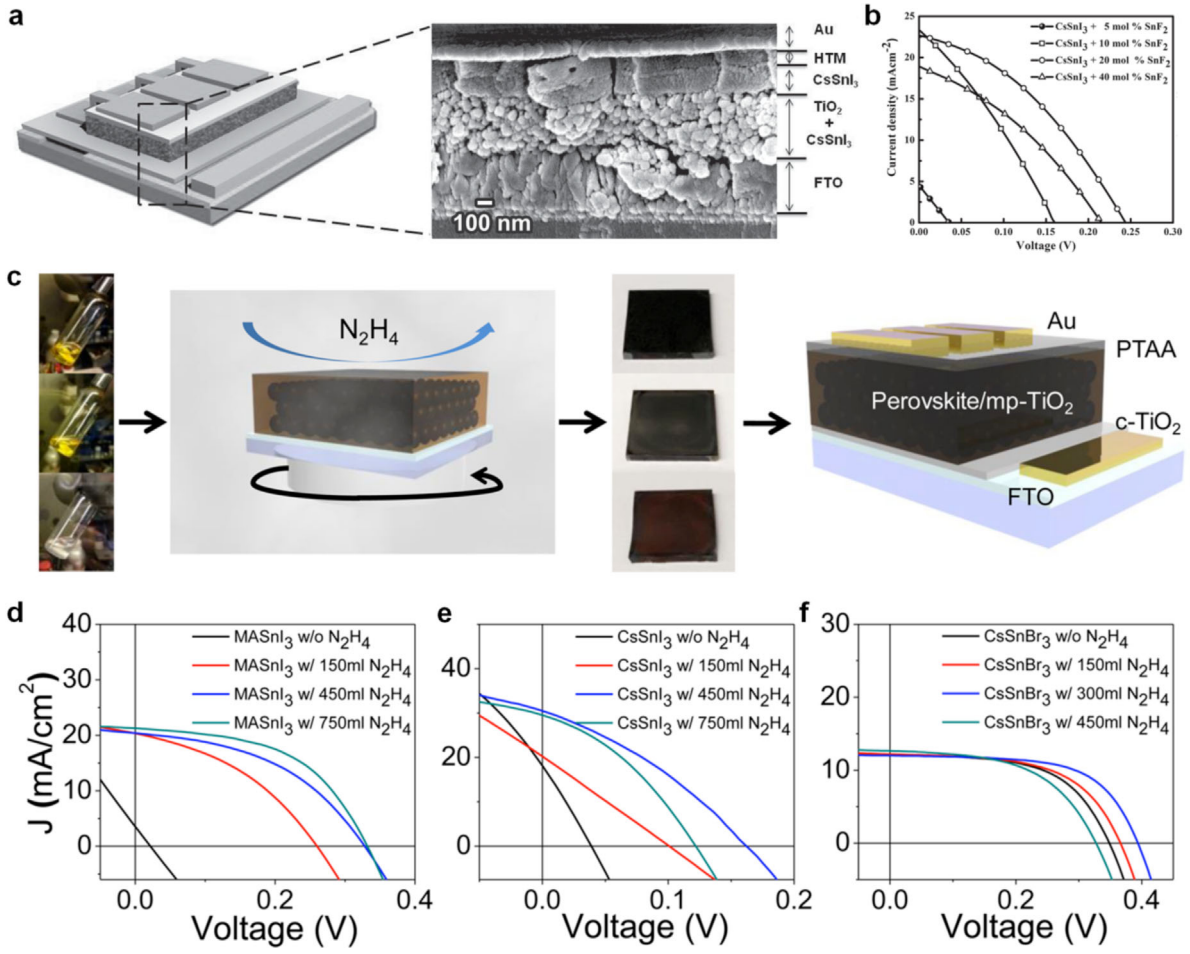

Figure 10. (a) Schematic and cross-section SEM image of the PSCs based on $CsSnI_3$. (b) *J–V* plots of the PSCs based on $CsSnI_3$ with and without SnF_2.[113] Copyright 2014, Wiley-VCH. (c) Reducing vapor atmosphere procedure for preparing PSCs and the device structure diagram; *J–V* plots of the PSCs based on (d) $MASnI_3$, (e) $CsSnI_3$ and (f) $CsSnBr_3$ with and without N_2H_4 treatment, respectively.[114] Copyright 2017, American Chemical Society.

vacancies and the fast oxidation of Sn^{2+} ions to Sn^{4+} ions when exposed in ambient atmosphere. Recently, several studies to improve the PCEs of the PSCs based on $CsSnX_3$ IMH perovskites have been reported. For example, Kumar et al. reported an improved performance by adding some SnF_2 into $CsSnI_3$ films to reduce the Sn-cation vacancies (**Figure 10**a–b).[113] Similar results were also obtained when SnF_2 was added into $CsSnBr_3$ IMH perovskites. The function of SnF_2 was demonstrated to reduce the Sn-cation vacancies. Moreover, Song et al. developed a reducing vapor atmosphere method by using hydrazine as the vapor to improve the quality of $CsSnX_3$ IMH perovskite films (Figure 10c).[114] As a result, improved PCEs were obtained for three kinds of PSCs (Figure 10d–f). The PCEs of the PSCs based on $CsSnX_3$ IMH perovskites was considered to have a lot of room for improvement. Wu et al. claimed that the PCEs of $CsSnI_3$ based PSCs may reach 23% by theoretical simulation.[117] Therefore, it is meaningful to pay more attentions into Sn-based IMH perovskites in the future studies.

In the end of this section, a summary of the PSCs based on IMH perovskites reported in the literatures are listed in **Table 2**. Overall, the PSCs based on IMH perovskites showed lower PCEs than those based on OMH perovskites. However, the performances of the PSCs based on IMH perovskites have been improving very rapidly since the first report published 2 years ago. Undoubtedly, it will be further enhanced in the near future.

3.2. Photodetectors

Similar with the PSCs, due to the super stability of the $CsPbBr_3$, most of the studies about PDs based on IMH perovskites focused on this material.[118–121] Li et al. developed a recyclable dissolution-recrystallization method to prepare uniform $CsPbBr_3$ films with crack-free, low-roughness surface for the application of PDs.[118] The dissolution process was occurred by adding several droplets of the mixture of ethanol and toluene on the as-prepared porous $CsPbBr_3$ film, and the recrystallization of $CsPbBr_3$ was induced when the solution evaporated (**Figure 11**a). After repeating this process for five times, the surface of porous $CsPbBr_3$ films become compact and uniform (Figure 11b–c). When used in PDs, the treated $CsPbBr_3$ films showed an obvious large current under the illumination of 442 nm (Figure 11d).

Table 2. Performance comparison of the PSCs based on IMH perovskites.

Materials	J_{SC} (mA cm^{-2})	V_{OC} (V)	FF	PCE (%)	References
$CsPbBr_3$	6.24	1.28	0.74	5.95	[59]
$CsPbBr_3$	6.7	1.25	0.73	6.2	[60]
$CsPbBr_3$	7.4	1.24	0.73	6.7	[62]
$CsPbIBr_2$	8.7	0.96	0.56	4.7	[79]
$CsPbIBr_2$	7.8	1.13	0.72	6.3	[110]
$CsPbI_2Br$	10.9	1.06	–	6.8	[74]
$CsPbI_2Br$	11.89	1.11	0.75	9.84	[78]
$CsPbI_2Br$	13.99	1.10	0.67	10.34	[111]
$Cs_{0.925}K_{0.075}PbI_2Br$	11.6	1.18	0.73	10.0	[112]
$CsPbI_3$	12	0.8	–	2.9	[107]
$CsPbI_3$	11.92	0.66	0.52	4.13	[108]
$CsPbI_3$	8.26	0.95	0.67	5.38	[109]
$CsPbI_3$	13.47	1.23	0.65	10.77	[65]
$CsSnI_3$	22.7	0.24	0.37	2.02	[113]
$CsSnI_3$	10.21	0.52	0.63	3.31	[115]
$CsSnBr_3$	13.96	0.37	0.59	3.04	[114]
$CsSnBr_3$	9.1	0.42	0.57	2.17	[116]

Moreover, the response rate of the treated $CsPbBr_3$ films was enhanced dramatically. The rise time and decay time decreased from 30 and 114 ms to 1 and 1.8 ms, respectively (Figure 11e). Finally, due to the excellent stability property of the $CsPbBr_3$ films, the PDs based on treated $CsPbBr_3$ films were stable for more than 2 months in ambient atmosphere.

As described in the section 2.3, $CsPbBr_3$ nanocrystals with various shapes, such as nanosheets/nanoplates, nanowires and so on, were successfully synthesized. The application of $CsPbBr_3$ nanocrystals in PDs has attracted great attention. Song et al. fabricated $CsPbBr_3$ nanosheets by modifying the hot-injection approach (**Figure 12**a).[122] Through simple ink-printing or roll-to-roll methods, crack-free $CsPbBr_3$ films with large area and high quality were prepared. Because of the strong light absorption and long carrier diffusion length of $CsPbBr_3$ nanosheets, the flexible PDs based on $CsPbBr_3$ films displayed an obvious increase in the current upon an illumination of 442 nm laser, showing a high on/off ratio of more than 10^3 and short rise/decay times (Figure 12b–d). Moreover, the flexible PDs exhibited good flexibility, maintaining a photocurrent comparable to the initial state after bending for 1000 times (Figure 12e), and showed high stability when exposed in ambient atmosphere.

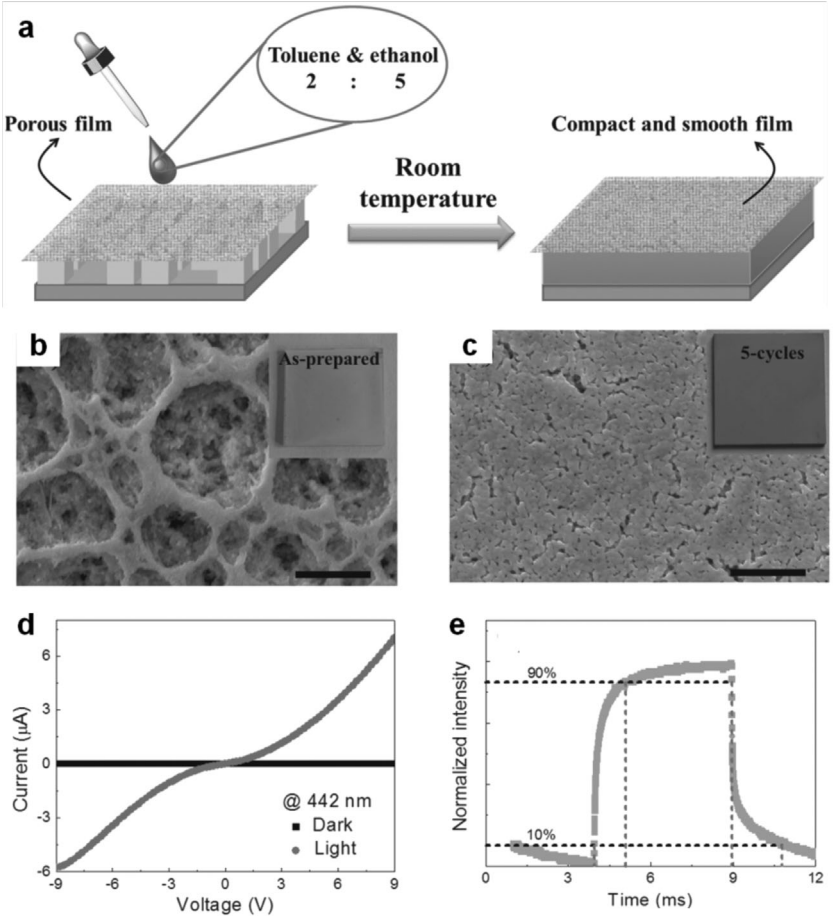

Figure 11. (a) Schematic of the dissolution-recrystallization treatment for $CsPbBr_3$ film. SEM images of $CsPbBr_3$ film (b) before and (c) after treated for five times. (d) *I–V* plots of the PD based on treated $CsPbBr_3$ film. (e) Photocurrent rise and decay time of PD based on treated $CsPbBr_3$ film at a light intensity of 1.01 mW cm^{-2}.[118] Copyright 2016, Wiley-VCH.

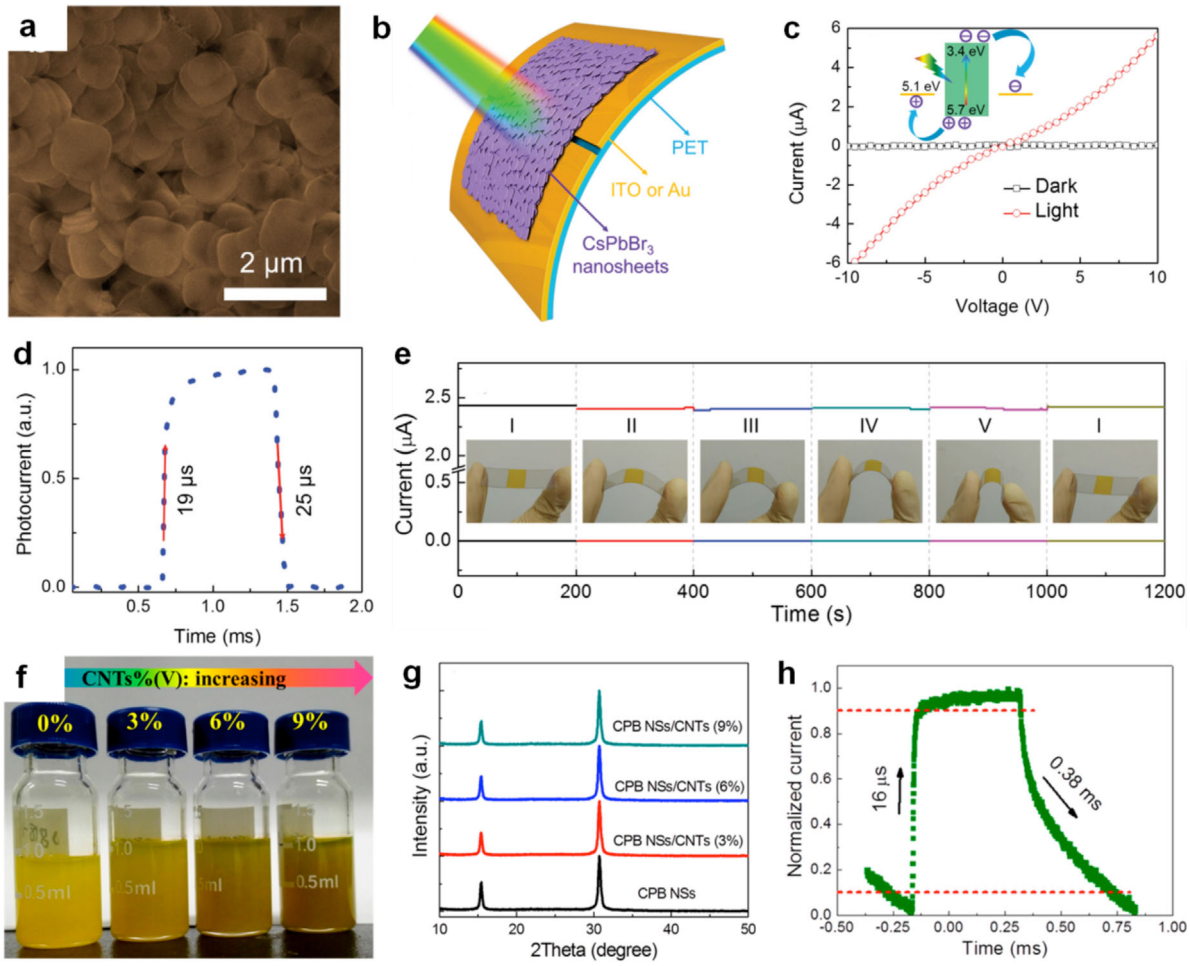

Figure 12. (a) SEM image of $CsPbBr_3$ nanosheets. (b) Schematic diagram of PDs based on $CsPbBr_3$ nanosheets. (c) *I–V* plots of the PDs based on $CsPbBr_3$ nanosheets. (d) Photocurrent rise and decay time of PD based on $CsPbBr_3$ nanosheets. (e) *I–t* plots of the flexible PDs bent at different angles.[122] Copyright 2016, Wiley-VCH. (f) Photograph of the $CsPbBr_3$ suspensions mixed with different amount of CNTs. (g) XRD patterns of the $CsPbBr_3$ films mixed with different amount CNTs. (h) Photocurrent rise time and decay time of PD based on $CsPbBr_3$/CNTs.[123] Copyright 2017, American Chemical Society.

To improve the performance of $CsPbBr_3$ based PDs, Li et al. presented a strategy of mixing carbon nanotubes (CNTs) and $CsPbBr_3$ together to boost the conductivity (Figure 12f–g).[123] As expected, the PDs based on $CsPbBr_3$/CNTs showed an external quantum efficiency (EQE) of 7488% and a photoresponsivity of 31.1 $A W^{-1}$, much higher than those based on $CsPbBr_3$ nanosheets (53% and 0.25 $A W^{-1}$). Due to the high conductivity, efficient charge extraction and transport, a shorter rise time of 16 μs was also obtained (Figure 12h). Moreover, similar with the PDs based on $CsPbBr_3$ nanosheets, the PDs based on $CsPbBr_3$ nanosheet/CNT composite still performed excellent flexibility.

Similar to $CsPbBr_3$ nanosheets, $CsPbBr_3$ nanowires were also used in PDs. Zhang et al. prepared uniform $CsPbBr_3$ nanowires by a modified hot-injection approach via anion-exchange reactions (**Figure 13**a).[124] The $CsPbBr_3$ nanowires with distinct compositions exhibited high PLQY ranging from 20% to 80%. To quantitatively study the level of defect density in $CsPbBr_3$ nanowires, PDs with the structure of Au/$CsPbX_3$ nanowires/Au were proposed (Figure 13b), which showed higher current when exposed under illumination (Figure 13c). Moreover, the photoresponse of this PD was fast and free of persistent photocurrent, which, combining the high PLQY, indicated that the existing defects in $CsPbX_3$ nanowires mainly form shallow traps (Figure 13d).

Apart from $CsPbBr_3$, the nanocrystals of other IMH perovskites (such as $CsPbI_3$) were also used for PDs. Ramasamy et al. prepared $CsPbI_3$ nanocrystal assembled films by anion exchange reactions (**Figure 14**a–b).[125] As mentioned in section 2.3, the $CsPbI_3$ nanocrystals obtained from the anion exchange reaction possessed the same phase and shape with the initial $CsPbBr_3$ nanocrystals. Under illumination, the photocurrent was increased by several orders of magnitude with the increase in light intensity, which resulted in a high on/off ratio of more than 10^5 (Figure 14c–d). In addition, the PDs based on $CsPbI_3$ nanocrystals exhibited fast rise time and decay time of 24 and 29 ms, respectively (Figure 14e–f).

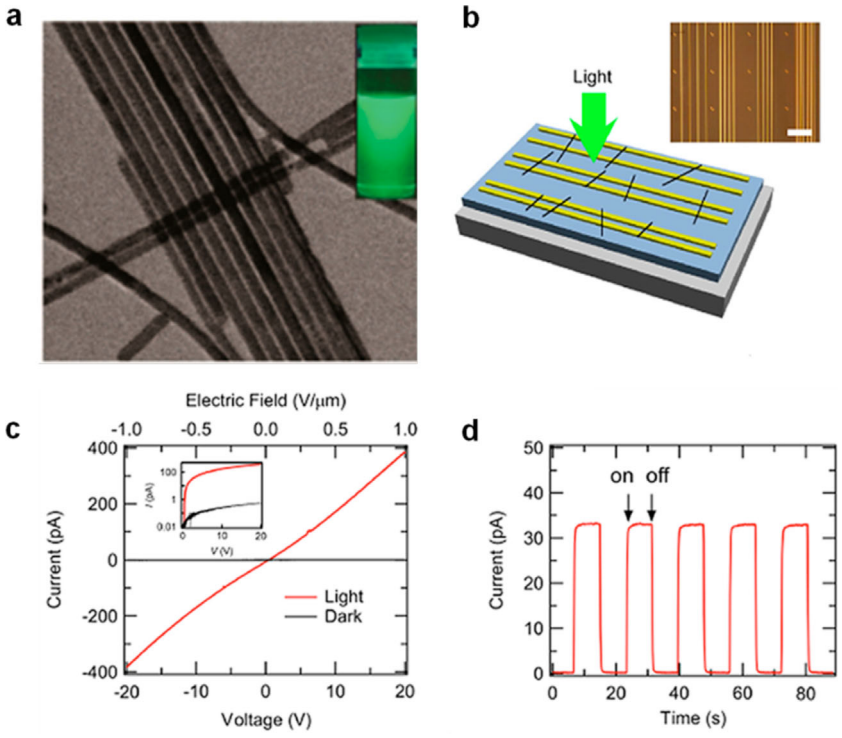

Figure 13. (a) SEM image of $CsPbBr_3$ nanowires. (b) Schematic diagram and (c) *I–V* plots of the PDs based on $CsPbBr_3$ nanowires. (d) Photoresponse of PDs based on $CsPbBr_3$ nanowires under a constant bias of 2.0 V.[124] Copyright 2016, American Chemical Society.

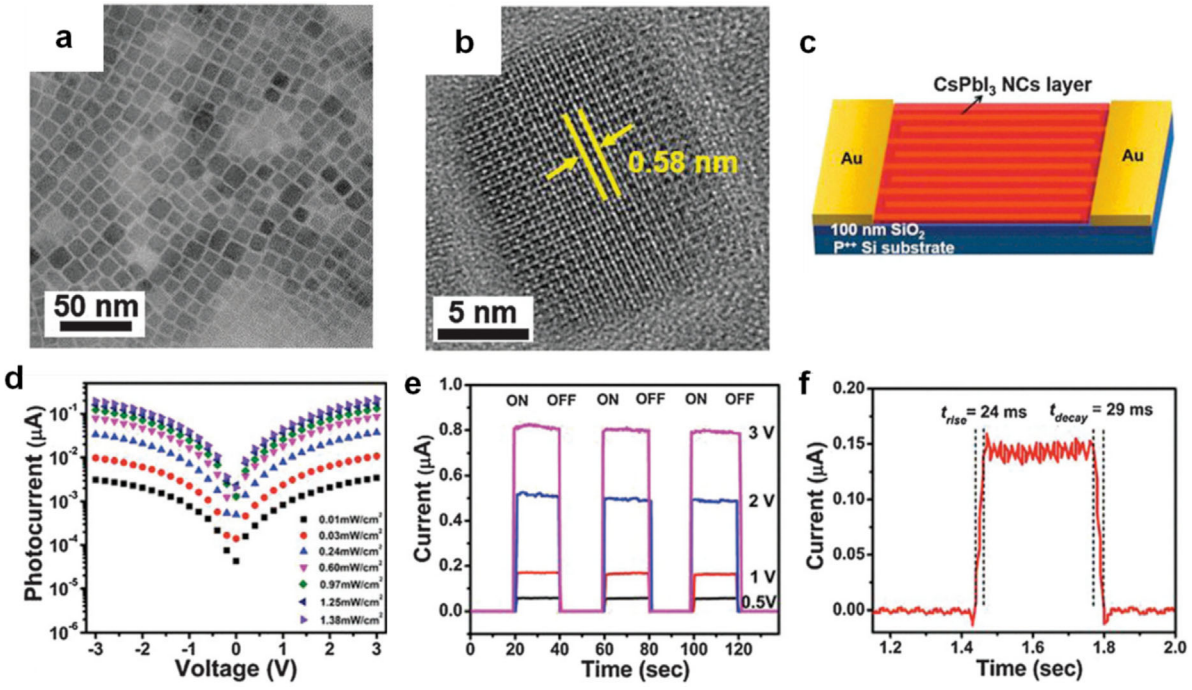

Figure 14. (a) TEM and (b) HRTEM images of $CsPbI_3$ nanocrystals. (c) Schematic diagram of the PDs based on $CsPbI_3$ nanocrystals. (d) *I–V* characteristics of PDs based on $CsPbI_3$ nanocrystals as a function of incident light intensity. (e) Photoresponse of PDs based on $CsPbI_3$ nanocrystals under different voltages. (f) Photocurrent rise time and decay time of PDs based on $CsPbI_3$ nanocrystals.[125] Copyright 2016, Royal Society of Chemistry.

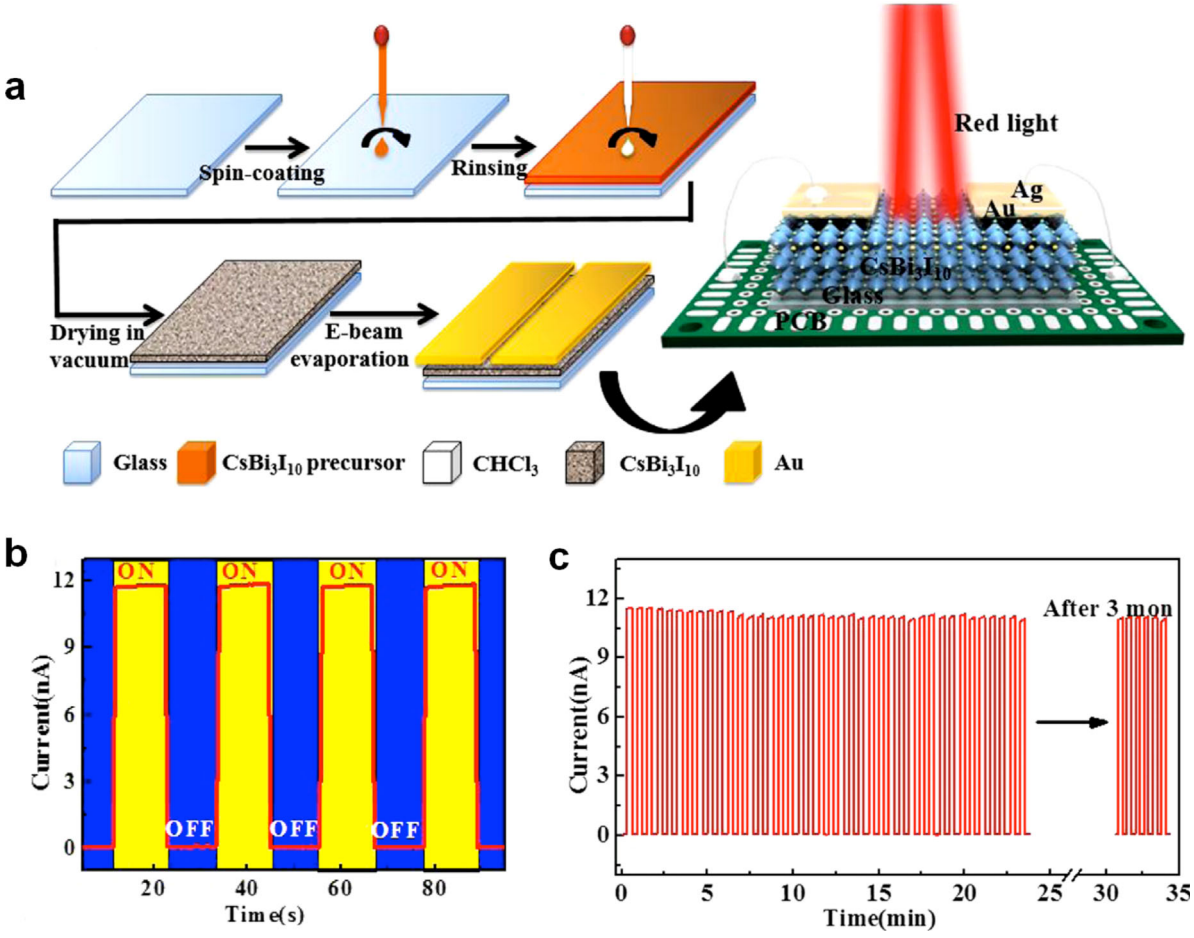

Figure 15. (a) Fabrication process of photodetectors based on $CsBi_3I_{10}$ perovskite films. (b) Photoresponse of $CsBi_3I_{10}$ based photodetectors under periodical light illumination of 650 nm wavelength at a bias voltage of 1.0 V. (c) Photoresponse of $CsBi_3I_{10}$ based photodetectors before and after 3 months.[126] Copyright 2017, American Chemical Society.

It is well known that Pb element is toxic and hazardous, therefore photodetectors based on lead-free inorganic halide perovskites has attracted great interests. For example, Tong et al. developed red-light sensitive photodetectors based on $CsBi_3I_{10}$ films, as shown in **Figure 15**a.[126] Because $CsBi_3I_{10}$ has a relatively narrow bandgap, the as-prepared photodetectors are sensitive to the light of 650 nm wavelength, with the rise and decay time of 0.33 and 0.38 ms, respectively (Figure 15b). Notably, the $CsBi_3I_{10}$ based photodetectors exhibited a very good stability even after storage for 3 months under ambient atmosphere (Figure 15c).

For comparison, the performances of the PDs based on IMH perovskites are listed in **Table 3**. Briefly, IMH perovskites have become on class of promising photo-sensing materials, owing to

Table 3. Performance comparison of the IMH perovskite based PDs.

Device structure	Responsivity ($A\,W^{-1}$)	On/off ratio	Rise time (ms)	Decay time (ms)	Stability	References
$Au/CsPbBr_3/Au$	0.18	8×10^3	1.8	1.0	>2 months	[118]
$Au/CsPbBr_3/Au$	2.1	4.6×10^2	~300	~300	–	[119]
$Au/TiO_2/CsPbBr_3/Au$	3.5	10^4	~ 10,000	~ 5000	–	[120]
$Au/CsPbBr_3/Au$	–	–	17.8	14.7	–	[121]
$ITO/CsPbBr_3/ITO$	0.64	$>10^4$	0.019	0.024	12 h	[122]
$ITO/CsPbBr_3$-CNTs/ITO	31.1	$>10^5$	0.016	0.38	–	[123]
$Au/CsPbBr_3/Au$	–	–	–	–	–	[124]
$Au/CsPbI_3/Au$	–	$>10^5$	24	29	–	[125]
$Au/CsBi_3I_{10}/Au$	21.8	10^5	0.33	0.38	>3 months	[126]

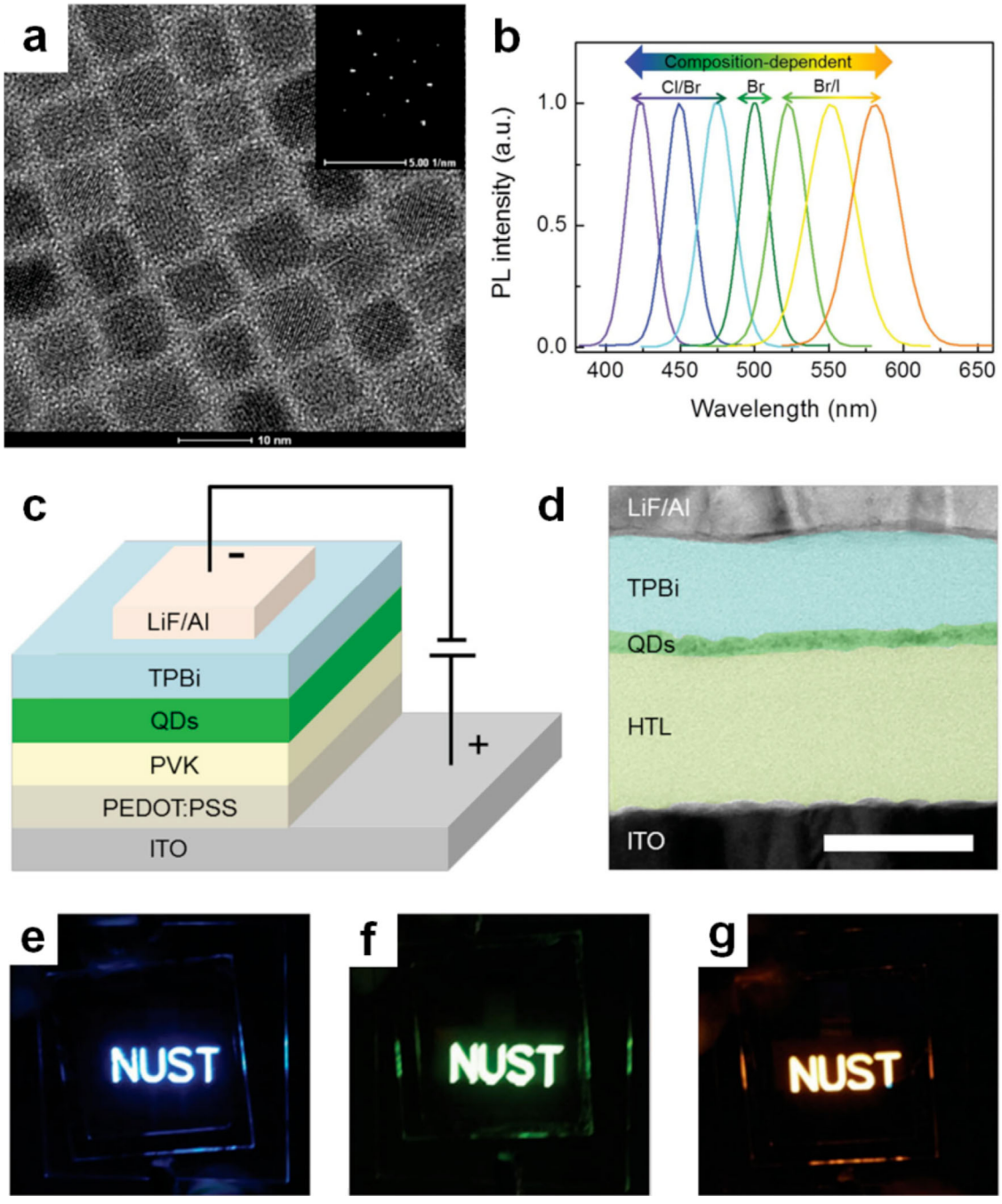

Figure 16. (a) TEM image of monodispersed perovskite nanocrystals. (b) Composition-tunable PL spectra of $CsPbX_3$ nanocrystals with different halides. (c) Schematic diagram, (d) cross-sectional SEM image and (e–g) Photographs of LEDs based on $CsPbX_3$ nanocrystals.[67] Copyright 2015, Wiley-VCH.

the large absorption coefficient, high charge carrier mobility, good stability, and so on. Therefore, it is valuable to make more efforts on the research of the PDs based on IMH perovskites.

3.3. Light-Emitting Diodes

Recently, IMH perovskites were also applied in the LED devices as light emitting materials.[67–70,127–136] Song et al. first reported the LEDs based on $CsPbX_3$ nanocrystals (**Figure 16**a–d).[67] In this work, three kinds of LEDs emitting blue, green, and organ light were fabricated with emission wavelength peaks at 455, 516, and 586 nm (Figure 16e–g). However, the performances of LEDs based on IMH perovskites are still inferior to those based on OMH perovskites, owing to low charging transporting resulted from the poor configuration of the LEDs and a mass of long ligands on the surface of $CsPbX_3$ nanocrystals. Therefore, to further improve the performances of LEDs based on IMH

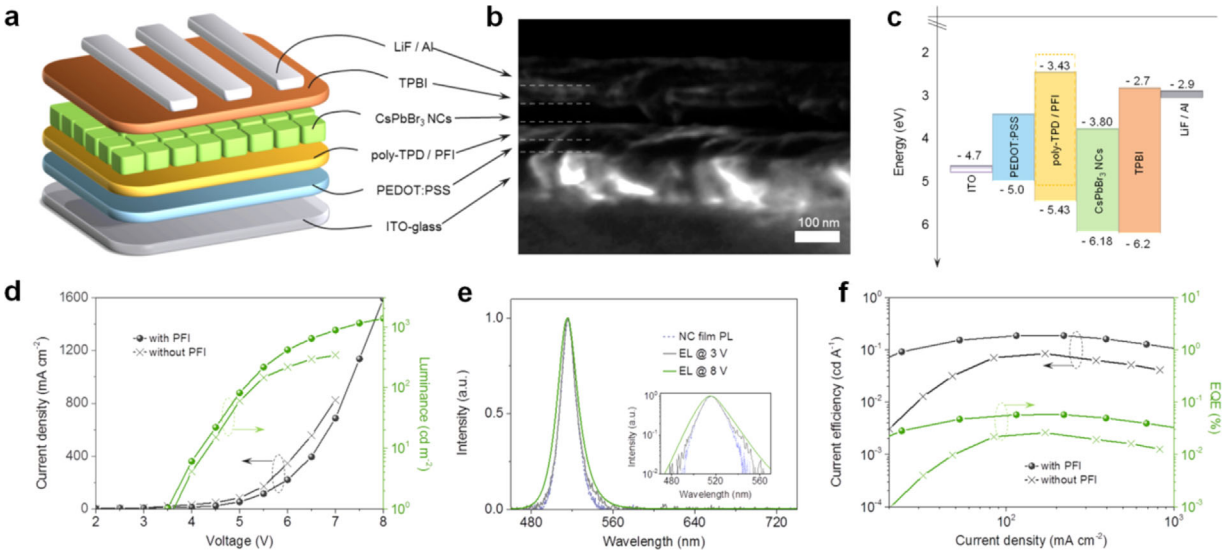

Figure 17. (a) Schematic structure, (b) cross-sectional SEM image and (c) band diagram of LEDs based on $CsPbBr_3$ nanocrystals. (d) Current density and brightness vs driving voltage (*J–I–V*) of LEDs with and without PFI. (e) PL spectrum of a $CsPbBr_3$ nanocrystal film, and EL spectra of LEDs with PFI at different voltages. (f) EQE and current efficiency vs current density of LEDs with and without PFI.[137] Copyright 2016, American Chemical Society.

perovskites, one possible way is to improve the charge transport properties by optimizing the configurations of LEDs, and another possible way is to improve the charge transport properties by reducing the amount of organic ligands on the surface of $CsPbX_3$ nanocrystals.

For the configurations of high-performance LEDs, one of the main obstacles is the existence of charge injection barrier between the charge-transporting layer and the emitter. To facilitate charge transportation, designing accordant charge-transporting layer and emitters is crucial, which can be addressed by introducing interfacial layers. Zhang et al. incorporated a perfluorinated ionomer (PFI) interlayer between the hole-transporting layer (poly TPD) and the $CsPbBr_3$ nanocrystal layer in the LEDs with ITO/poly TPD/$CsPbBr_3$/TPBI/LiF/Al structure.[137] The PFI interlayer led to a 0.34 eV increase of VBM of poly TPD, providing a more matching band

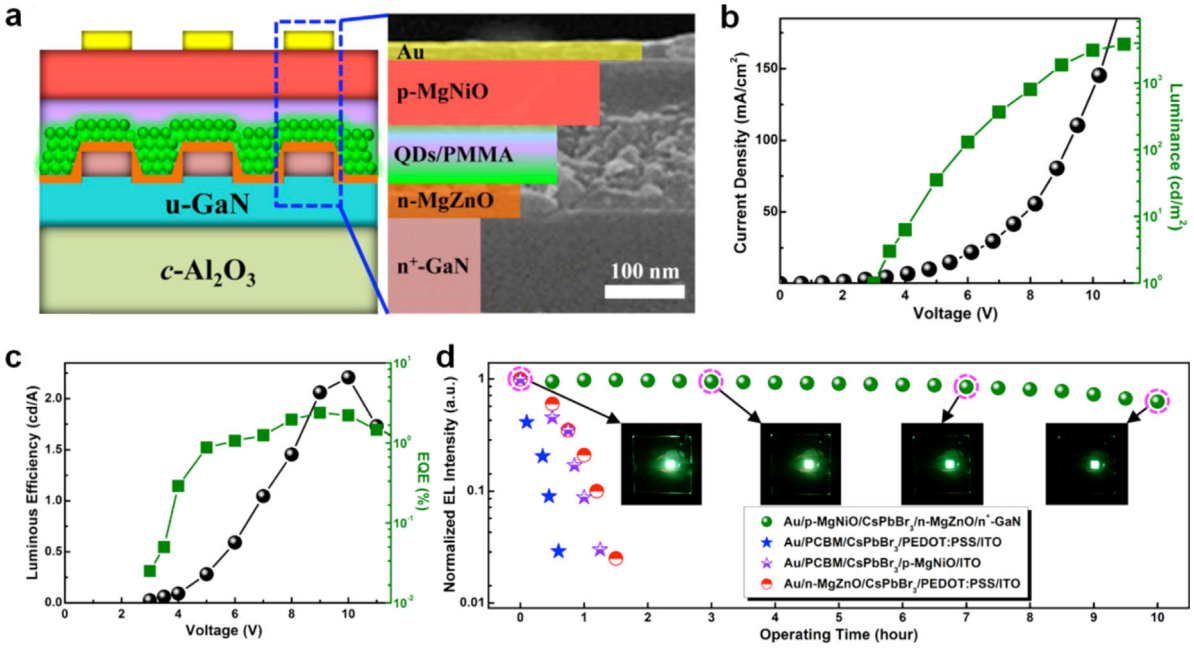

Figure 18. (a) Schematic structure and cross-sectional SEM image of $CsPbBr_3$ based LEDs. (b) *J–I–V* plots, (c) EQE and current efficiency vs current density plots of $CsPbBr_3$ based LEDs. (d) Emission intensity of the four kinds of LEDs as a function of running time under a continuous bias of 10.0 V.[138] Copyright 2016, American Chemical Society.

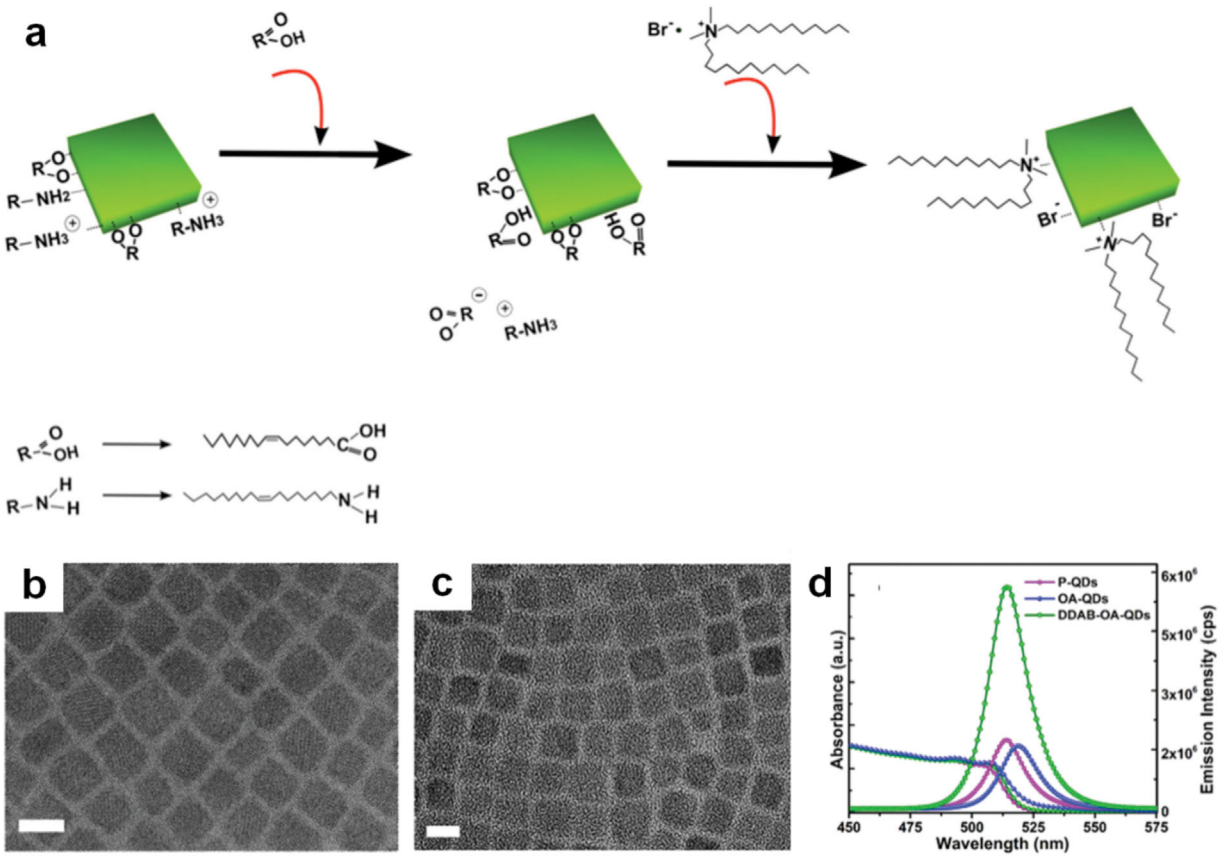

Figure 19. (a) The ligand-exchange mechanism on $CsPbX_3$ nanocrystal surface. (b) SEM images of (b) untreated and (c) treated $CsPbX_3$ nanocrystals (scale bars: 10 nm). (d) PL spectra of the three samples (untreated, treated, and treated by the intermediate step).[139] Copyright 2016, Wiley-VCH.

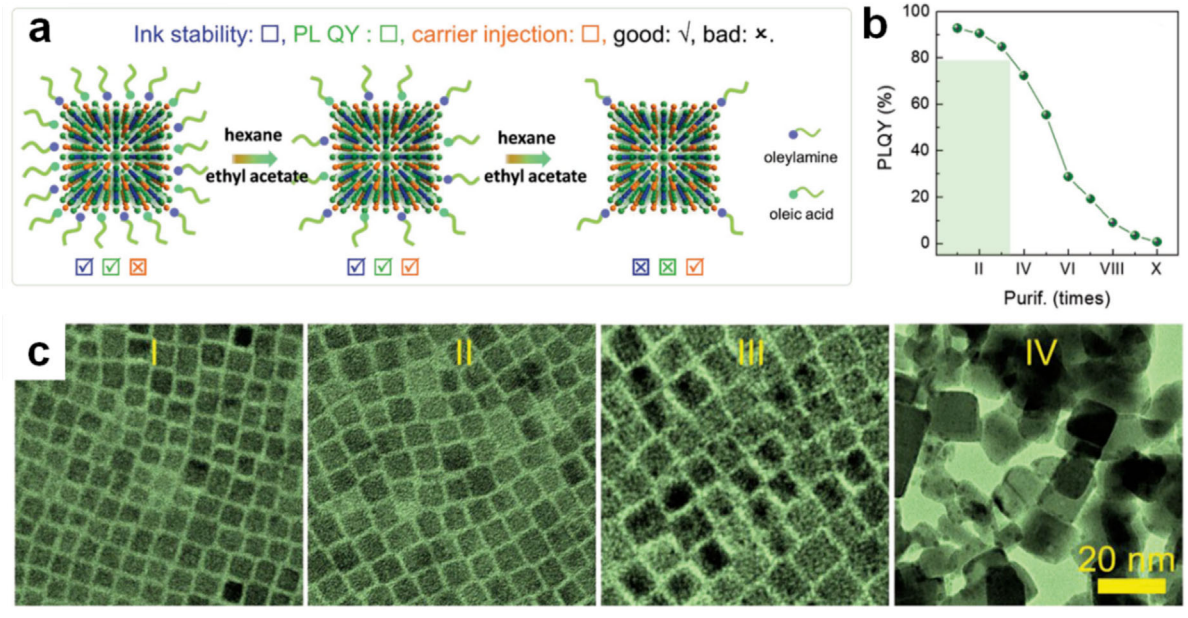

Figure 20. (a) Schematic illustration of the control of ligand density on $CsPbBr_3$ nanocrystal surface. (b) PLQY of $CsPbBr_3$ nanocrystal inks after different purification cycles dispersed in hexane. (c) TEM images of $CsPbBr_3$ nanocrystals after different numbers of purification cycles.[72] Copyright 2016, Wiley-VCH.

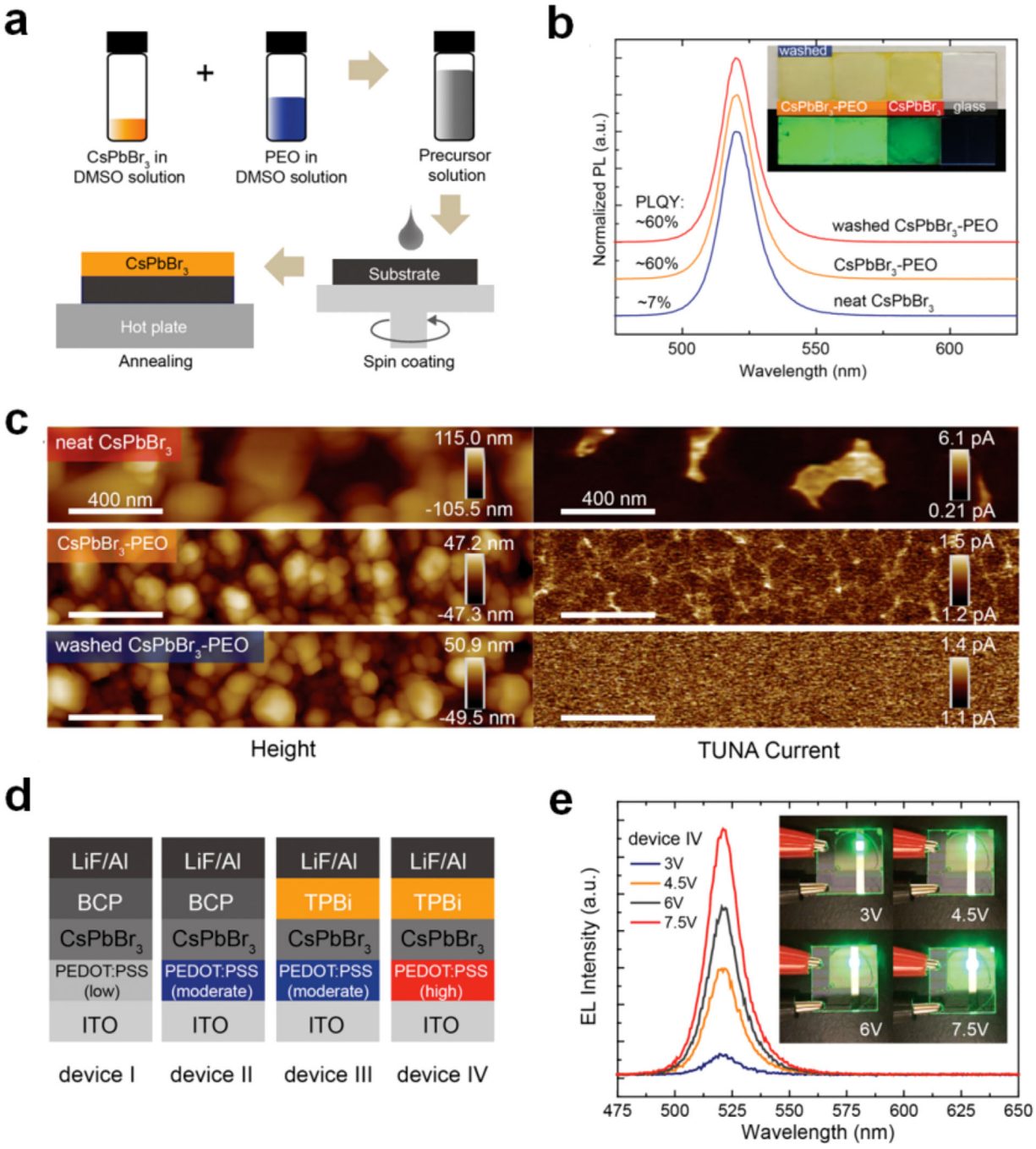

Figure 21. (a) The preparation process of $CsPbBr_3$ thin films. (b) PL spectra of three kinds of $CsPbBr_3$ thin films. (c) In situ local electrical current and film topography mappings. (d) Schematic diagrams of $CsPbBr_3$ based LEDs. (e) Emission from device IV shows stable EL spectra as the voltage increases.[140] Copyright 2016, Wiley-VCH.

structure with $CsPbBr_3$ (**Figure 17**a–c). The PFI layer was also beneficial to maintain the charge balance of $CsPbBr_3$ nanocrystal layer and preserve the emissive properties. As a result, bright green emission could be observed from the modified LEDs, and exhibiting improved parameters, such as low turn-on voltage, strong peak luminance, and high EQE compared to those without PFI layer (Figure 17d–f). Unfortunately, the LEDs still showed unstable electroluminescence, and the signal decayed to 50% of its initial value after 10 min. It indicates that for optimizing the configuration of IMH perovskite LEDs, both the matching of band structures and the stability of emitting layer should be considered. To address these two issues, Shi et al. proposed an all-inorganic LED with the structure of c-Al_2O_3/n^+-GaN/MgZnO/$CsPbBr_3$/PMMA/MgNiO/Au, in which MgZnO

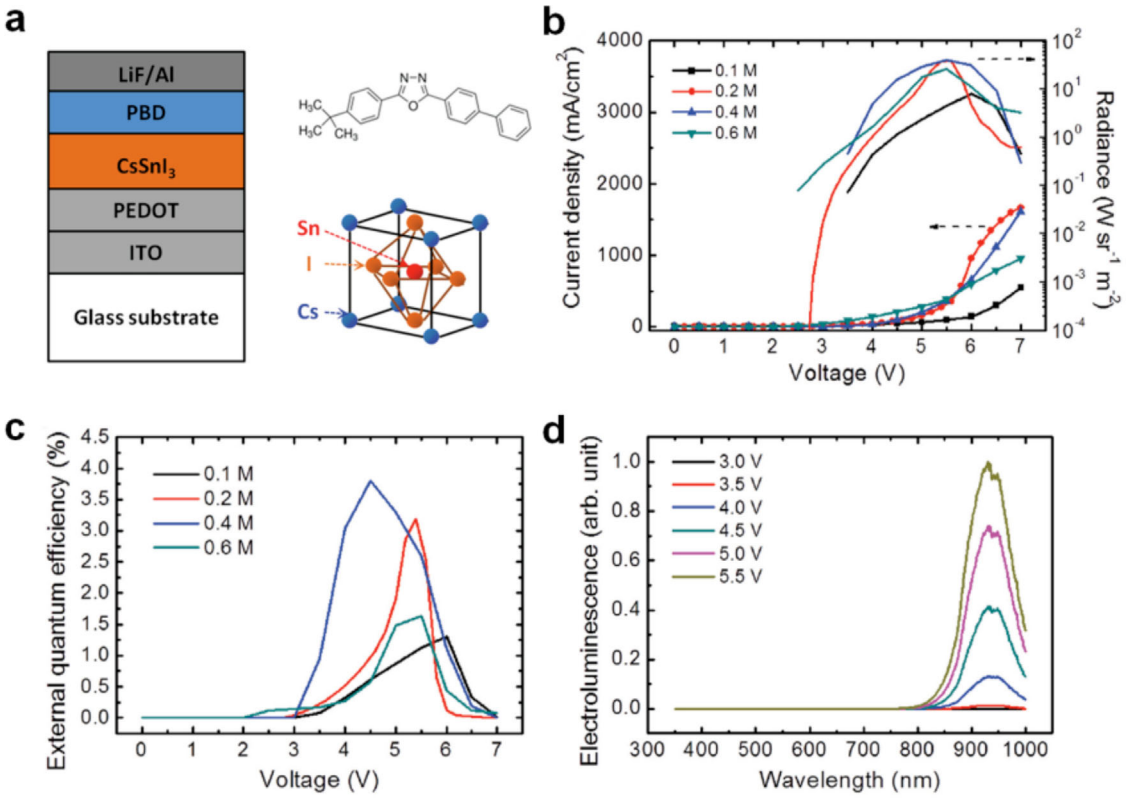

Figure 22. (a) Schematic diagram of the LEDs based on $CsSnI_3$ films. (b) *J–I–V* plots, (c) EQE plots, and (d) EL plots of the LEDs based on $CsSnI_3$ films.[141] Copyright 2016, Wiley-VCH.

Table 4. Performance comparison of the LEDs based on IMH perovskites.

Materials	EL λ_{max} (nm)	V_{on} (V)	Max. EQE (%)	Max. CE (cd A^{-1})	Max. PE (lm W^{-1})	Max. L (cd m^{-2})	References
$CsPbBr_3$	517	5.8	0.35	1.2	–	2938	[127]
$CsPbI_3$	698	–	5.7	–	–	206	[128]
$CsPbI_{2.25}Br_{0.75}$	619	–	1.4	–	–	1559	[128]
$CsPbBr_3$	523	–	0.19	–	–	2335	[128]
$CsPbBr_{1.5}Cl_{1.5}$	480	–	0.0074	–	–	8.7	[128]
$CsPbBr_3$-CsBr	524	2.8	0.15	0.57	–	7276	[131]
$CsPbBrxI_{3-x}$	–	4.0	–	0.027	0.021	21.7	[133]
$CsPbBr_3$	–	5.0	–	0.308	0.16	51.7	[133]
$CsPbBr_xCl_{3-x}$	–	4.0	–	0.025	0.019	15.2	[133]
$CsPbBr_3$-$CsPb_2Br_5$	527	4.6	2.21	8.98	3.4	3853	[68]
$CsPb(Br/I)_3$	586	4.6	0.09	0.08	0.06	528	[67]
$CsPbBr_3$	516	4.2	0.12	0.43	0.18	946	[67]
$CsPb(Br/Cl)_3$	455	5.1	0.07	0.14	0.07	742	[67]
$CsPbBr_3$	516	3.5	0.06	0.19	–	1377	[137]
$CsPbBr_3$	522	3.0	2.39	2.25	–	3809	[138]
$CsPbBr_3$	515	3.0	3.0	–	–	330	[139]
$CsPbBr_xCl_{3-x}$	490	3.0	1.9	–	–	35	[139]
$CsPbBr_3$	512	3.4	6.27	13.3	5.24	15,185	[72]
$CsPbBr_3$	521	2.5	4.26	15.67	–	53,525	[140]
$CsSnI_3$	950	–	3.8	–	–	–	[141]

and MgNiO were used as the electron and hole injectors, respectively (**Figure 18**a).[138] The band structures of MgZnO and MgNiO can be engineered by adjusting the ratios of Mg^{2+} ions. As a result, the LEDs exhibited the luminance, luminous efficiency, and EQE as high as 3809 cd m^{-2}, 2.25 cd A^{-1}, and 2.39%, respectively (Figure 18b–c). Moreover, the LEDs can retain nearly 80% of the initial efficiency when operated continually for 10 h under 10.0 V, indicating a significantly improvement on operation stability (Figure 18d).

For the amount of long ligands, they have double side effects in the application of LEDs. The long ligands on the surface of $CsPbX_3$ nanocrystals can provide sufficient surface passivation and result in high PLQYs and ink stability. However, insulating long ligands capped on $CsPbX_3$ nanocrystals may hinder the charge transport. Therefore, controlling the amount of long ligands on $CsPbX_3$ nanocrystal surface can balance the surface passivation and charge transport. Pan et al. demonstrated the replacement of long ligands with shorter ligands, such as di-dodecyl dimethyl ammonium bromide (DDAB), to enhance the charge transport of $CsPbBr_3$ films (**Figure 19**a).[139] The results showed the treated $CsPbBr_3$ nanocrystals can preserve the original particle sizes and shapes, and the PLQY increased from 49% to 71% (Figure 19b–d). When used in LEDs, the treated $CsPbBr_3$ nanocrystals exhibited a sharp EL peak with high luminance and high EQE. Simply, Li et al. pointed out that the ligand density can be controlled just by washing the $CsPbBr_3$ nanocrystals with hexane/ethyl acetate mixed solvent (**Figure 20**a).[72] By adjusting the washing times, the $CsPbBr_3$ nanocrystals can persevere the initial shapes and sizes, and exhibit a high PLQY (Figure 20b–c). When the $CsPbBr_3$ nanocrystals washed for two times were employed into LEDs, a high EQE of 6.27% and current efficiency of 13.3 cd A^{-1} were achieved.

To completely avoid the negative effect of capping ligands, preparing $CsPbX_3$ thin film using the one-step solution process is a possible method, however, the low solubility of CsBr precursor makes it difficult to obtain high-quality $CsPbBr_3$ thin films. To resolve this problem, Ling et al. proposed a new synthetic method by dissolving poly(ethylene oxide) (PEO) and $CsPbBr_3$ in DMSO to fabricate microcrystalline $CsPbBr_3$ films followed by washing in chlorobenzene (**Figure 21**a),[140] showing higher PLQY and better morphology than pristine $CsPbBr_3$ films (Figure 21b–c). In this work, four different kinds of LEDs based on modified $CsPbBr_3$ films were fabricated (Figure 21d). Among them, the device IV exhibited the maximum luminance, EQE, and current efficiency of 53525 cd m^{-2}, 4.26%, and 15.67 cd A^{-1}, respectively (Figure 21d–e). This study proved once again that besides the amount of long ligands, the configuration of LED is also crucial for the performances.

LEDs based on other IMH perovskites, such as $CsSnX_3$, were also fabricated. Hong et al. fabricated infrared LEDs based on uniform, dense $CsSnI_3$ films prepared via a low-temperature solution process (**Figure 22**a).[141] The infrared LEDs displayed high performances with an EL peak at 950 nm, maximum radiance of 40 W/sr m^{-2} at a current of 364.3 mA cm^{-2} and a maximum EQE of 3.8% at 4.5 V, respectively (Figure 22c–d).

For comparison, a summary of the LEDs based on IMH perovskites are listed in **Table 4**. Owing to the remarkable optoelectronic properties, the LEDs based on IMH perovskites are developing rapid. As mentioned above, the EQE of LEDs based on $CsPbBr_3$ has raised from 0.12% to 6.27% in less than 2 years. Similar to PSCs and PDs, the LEDs based on IMH perovskites have a promising future as well.

4. Conclusions and Outlook

In summary, here we reviewed the recent advances of IMH perovskites, especially the synthesis methods, modification strategies and the potential applications in varied optoelectronic devices, including PSCs, PDs, and LEDs. However, compared with OMH perovskites, the performances of IMH perovskite based devices are still not very desirable. Just like a coin has two sides, the relative low performances and the short developing time indicate there is still plenty of room for the research of IMH perovskites.

Compared with OMH perovskites, the IMH perovskites, such as $CsPbBr_3$, exhibited higher stability. However, the bandgaps of IMH perovskites usually are not very appropriate for the application in PSCs, therefore the engineering of bandgap is necessary. Recently, the PCE of IMH perovskite based PSCs has raised from 6% to ~11%. Unfortunately, although the modified IMH perovskites exhibited higher PCEs, their stability was usually poorer than $CsPbBr_3$, especially in humid atmosphere. This drawback was also found in the applications of PDs and LEDs. Therefore, it is required to find more optimized solutions to adjust the bandgaps and improve the stability simultaneously.

On the other hand, IMH perovskites are more appropriate to be utilized in silicon-perovskite tandem solar cells, which is very promising for industrial application. The bandgap of crystalline Si is about 1.1 eV. To obtain an optimized overall PCE for the silicon-perovskite tandem solar cells, a bandgap of ~1.75 eV is required for the IMH perovskites to absorb light as much as possible.[21,107] For example, the bandgaps of $CsPbBr_3$ and $CsPbI_3$ are 2.3 and 1.73 eV, respectively, which indicates the bandgap of $CsPbI_xBr_{3-x}$ can be tuned between 1.73–2.3 eV by adjusting the halide compositions. Therefore, employing IMH perovskites into the silicon-perovskite tandem devices is possible.

Meanwhile, strengthening the basic theoretical research of IMH perovskites is necessary as well. To date, many experimental results on IMH perovskites have been reported, however, systematic theoretical simulations on them are not enough. For example, the PSCs based on $CsPbI_2Br$ exhibited rising device performance under continuous illumination,[106] which was ascribed to the enhancement of hole collection by a series of experimental characterizations, however, no theoretical clarification was developed to explain this result. Therefore, it is desirable to establish suitable theoretical models for IMH perovskites.

Similar with OMH perovskites, the research of Pb-based IMH perovskites is still the mainstream, which are toxic and harmful. Non-toxic lead-free IMH perovskites with good properties are more preferable. Optoelectronic devices based on lead-free IMH perovskites (e.g., $CsSnX_3$) have been studied recently. However, the performances were usually lower than those based on Pb-based IMH perovskites, and more systematic researches are required. Overall, the IMH perovskites have had rapid progress within recent 2 years and exhibited great potential for optoelectronic applications, while more efforts are still needed to optimize the properties.

Acknowledgments

This work is supported by National Key Research and Development Program of China (2017YFA0208200, 2016YFB0700600), National Key Basic Research Program (2015CB659300), Programs of NSFC (21403105, 21573108), China Postdoctoral Science Foundation (2015M580412), Natural Science Foundation of Jiangsu Province (BK20160647), Fundamental Research Funds for the Central Universities (020514380107), and a project funded by the Priority Academic Program Development of Jiangsu Higher Education Institutions.

Conflicts of Interest

The authors declare no conflict of interest.

Keywords

inorganic perovskites, optoelectronic devices, perovskite solar cells, photodetectors, light-emitting diodes

Received: May 30, 2017
Revised: July 16, 2017
Published online: August 31, 2017

[1] J. Burschka, N. Pellet, S.-J. Moon, R. Humphry-Baker, P. Gao, M. K. Nazeeruddin, M. Graetzel, *Nature* **2013**, *499*, 316.
[2] M. Liu, M. B. Johnston, H. J. Snaith, *Nature* **2013**, *501*, 395.
[3] D. W. deQuilettes, S. M. Vorpahl, S. D. Stranks, H. Nagaoka, G. E. Eperon, M. E. Ziffer, H. J. Snaith, D. S. Ginger, *Science* **2015**, *348*, 683.
[4] Q. Dong, Y. Fang, Y. Shao, P. Mulligan, J. Qiu, L. Cao, J. Huang, *Science* **2015**, *347*, 967.
[5] Z. Guo, Y. Wan, M. Yang, J. Snaider, K. Zhu, L. Huang, *Science* **2017**, *356*, 59.
[6] W. Nie, H. Tsai, R. Asadpour, J.-C. Blancon, A. J. Neukirch, G. Gupta, J. J. Crochet, M. Chhowalla, S. Tretiak, M. A. Alam, H.-L. Wang, A. D. Mohite, *Science* **2015**, *347*, 522.
[7] D. Shi, V. Adinolfi, R. Comin, M. Yuan, E. Alarousu, A. Buin, Y. Chen, S. Hoogland, A. Rothenberger, K. Katsiev, Y. Losovyj, X. Zhang, P. A. Dowben, O. F. Mohammed, E. H. Sargent, O. M. Bakr, *Science* **2015**, *347*, 519.
[8] S. D. Stranks, G. E. Eperon, G. Grancini, C. Menelaou, M. J. P. Alcocer, T. Leijtens, L. M. Herz, A. Petrozza, H. J. Snaith, *Science* **2013**, *342*, 341.
[9] B. Turan, A. Huuskonen, I. Kuhn, T. Kirchartz, S. Haas, *Solar RRL* **2017**, *1*, 1700003.
[10] Y. Sun, X. Yan, *Solar RRL* **2017**, *1*, 1700002.
[11] G. Xing, N. Mathews, S. Sun, S. S. Lim, Y. M. Lam, M. Graetzel, S. Mhaisalkar, T. C. Sum, *Science* **2013**, *342*, 344.
[12] J.-Y. Jeng, Y.-F. Chiang, M.-H. Lee, S.-R. Peng, T.-F. Guo, P. Chen, T.-C. Wen, *Adv. Mater.* **2013**, *25*, 3727.
[13] J.-Y. Jeng, K.-C. Chen, T.-Y. Chiang, P.-Y. Lin, T.-D. Tsai, Y.-C. Chang, T.-F. Guo, P. Chen, T.-C. Wen, Y.-J. Hsu, *Adv. Mater.* **2014**, *26*, 4107.
[14] B. Conings, L. Baeten, C. De Dobbelaere, J. D'Haen, J. Manca, H.-G. Boyen, *Adv. Mater.* **2014**, *26*, 2041.
[15] J.-H. Im, I.-H. Jang, N. Pellet, M. Graetzel, N.-G. Park, *Nature Nanotech.* **2014**, *9*, 927.
[16] N. J. Jeon, J. H. Noh, W. S. Yang, Y. C. Kim, S. Ryu, J. Seo, S. I. Seok, *Nature* **2015**, *517*, 476.
[17] H. Tsai, W. Nie, J.-C. Blancon, C. C. Stoumpos, R. Asadpour, B. Harutyunyan, A. J. Neukirch, R. Verduzco, J. J. Crochet, S. Tretiak, L. Pedesseau, J. Even, M. A. Alam, G. Gupta, J. Lou, P. M. Ajayan, M. J. Bedzyk, M. G. Kanatzidis, *Nature* **2016**, *536*, 312.
[18] F. Bella, G. Griffini, J.-P. Correa-Baena, G. Saracco, M. Gratzel, A. Hagfeldt, S. Turri, C. Gerbaldi, *Science* **2016**, *354*, 203.
[19] W. Chen, Y. Wu, Y. Yue, J. Liu, W. Zhang, X. Yang, H. Chen, E. Bi, I. Ashraful, M. Graetzel, L. Han, *Science* **2015**, *350*, 944.
[20] L. Dou, A. B. Wong, Y. Yu, M. Lai, N. Kornienko, S. W. Eaton, A. Fu, C. G. Bischak, J. Ma, T. Ding, N. S. Ginsberg, L.-W. Wang, A. P. Alivisatos, P. Yang, *Science* **2015**, *349*, 1518.
[21] G. E. Eperon, T. Leijtens, K. A. Bush, R. Prasanna, T. Green, J.T.-W. Wang, D. P. McMeekin, G. Volonakis, R. L. Milot, R. May, A. Palmstrom, D. J. Slotcavage, R. A. Belisle, J. B. Patel, E. S. Parrott, R. J. Sutton, W. Ma, F. Moghadam, B. Conings, A. Babayigit, H.-G. Boyen, S. Bent, F. Giustino, L. M. Herz, M. B. Johnston, M. D. McGehee, H. J. Snaith, *Science* **2016**, *354*, 861.
[22] M. M. Lee, J. Teuscher, T. Miyasaka, T. N. Murakami, H. J. Snaith, *Science* **2012**, *338*, 643.
[23] X. Li, D. Bi, C. Yi, J.-D. Decoppet, J. Luo, S. M. Zakeeruddin, A. Hagfeldt, M. Gratzel, *Science* **2016**, *353*, 58.
[24] D. P. McMeekin, G. Sadoughi, W. Rehman, G. E. Eperon, M. Saliba, M. T. Hoerantner, A. Haghighirad, N. Sakai, L. Korte, B. Rech, M. B. Johnston, L. M. Herz, H. J. Snaith, *Science* **2016**, *351*, 151.
[25] A. Mei, X. Li, L. Liu, Z. Ku, T. Liu, Y. Rong, M. Xu, M. Hu, J. Chen, Y. Yang, M. Graetzel, H. Han, *Science* **2014**, *345*, 295.
[26] H. Tan, A. Jain, O. Voznyy, X. Lan, F. P. G. de Arquer, J. Z. Fan, R. Quintero-Bermudez, M. Yuan, B. Zhang, Y. Zhao, F. Fan, P. Li, L. N. Quan, Y. Zhao, Z.-H. Lu, Z. Yang, S. Hoogland, E. H. Sargent, *Science* **2017**, *355*, 722.
[27] H. Zhou, Q. Chen, G. Li, S. Luo, T.-B. Song, H.-S. Duan, Z. Hong, J. You, Y. Liu, Y. Yang, *Science* **2014**, *345*, 542.
[28] W. S. Yang, J. H. Noh, N. J. Jeon, Y. C. Kim, S. Ryu, J. Seo, S. I. Seok, *Science* **2015**, *348*, 1234.
[29] Y. Hu, S. Si, A. Mei, Y. Rong, H. Liu, X. Li, H. Han, *Solar RRL* **2017**, *1*, 1600019.
[30] H. Lei, G. Yang, X. Zheng, Z. Zhang, C. Chen, J. Ma, Y. Guo, Z. Chen, P. Qin, Y. Li, G. Fang, *Solar RRL* **2017**, *1*, 1700038.
[31] H. Cho, S.-H. Jeong, M.-H. Park, Y.-H. Kim, C. Wolf, C.-L. Lee, J. H. Heo, A. Sadhanala, N. Myoung, S. Yoo, S. H. Im, R. H. Friend, T.-W. Lee, *Science* **2015**, *350*, 1222.
[32] Y.-H. Kim, H. Cho, J. H. Heo, T.-S. Kim, N. Myoung, C.-L. Lee, S. H. Im, T.-W. Lee, *Adv. Mater.* **2015**, *27*, 1248.
[33] A. Nurmikko, *Nature Nanotech.* **2015**, *10*, 1001.
[34] S. D. Stranks, H. J. Snaith, *Nature Nanotechnol.* **2015**, *10*, 391.
[35] M. Yuan, Q. Li Na, R. Comin, G. Walters, R. Sabatini, O. Voznyy, S. Hoogland, Y. Zhao, E. M. Beauregard, P. Kanjanaboos, Z. Lu, D. H. Kim, E. H. Sargent, *Nature Nanotechnol.* **2016**, *11*, 872.
[36] R. Dong, Y. Fang, J. Chae, J. Dai, Z. Xiao, Q. Dong, Y. Yuan, A. Centrone, X. C. Zeng, J. Huang, *Adv. Mater.* **2015**, *27*.
[37] Y. Lee, J. Kwon, E. Hwang, C.-H. Ra, W. J. Yoo, J.-H. Ahn, J. H. Park, J. H. Cho, *Adv. Mater.* **2015**, *27*, 41.
[38] L. Dou, Y. Yang, J. You, Z. Hong, W.-H. Chang, G. Li, Y. Yang, *Nature Commun.* **2014**, *5*, 5405.
[39] Y. Fang, Q. Dong, Y. Shao, Y. Yuan, J. Huang, *Nature Photon.* **2015**, *9*, 679.
[40] N. Tsvetkov, Q. Lu, L. Sun, E. J. Crumlin, B. Yildiz, *Nature Mater.* **2016**, *15*, 1010.
[41] J. You, L. Meng, T.-B. Song, T.-F. Guo, Y. Yang, W.-H. Chang, Z. Hong, H. Chen, H. Zhou, Q. Chen, Y. Liu, N. De Marco, Y. Yang, *Nature Nanotechnol.* **2016**, *11*, 75.
[42] Y. Yang, J. You, *Nature* **2017**, *544*, 155.
[43] N. Ahn, K. Kwak, M. S. Jang, H. Yoon, B. Y. Lee, J.-K. Lee, P. V. Pikhitsa, J. Byun, M. Choi, *Nature Commun.* **2016**, *7*, 13422.
[44] Y. Bai, Q. Dong, Y. Shao, Y. Deng, Q. Wang, L. Shen, D. Wang, W. Wei, J. Huang, *Nature Commun.* **2016**, *7*, 12806.

[45] K. O. Brinkmann, J. Zhao, N. Pourdavoud, T. Becker, T. Hu, S. Olthof, K. Meerholz, L. Hoffmann, T. Gahlmann, R. Heiderhoff, M. F. Oszajca, N. A. Luechinger, D. Rogalla, Y. Chen, B. Cheng, T. Riedl, *Nature Commun.* **2017**, *8*, 13938.
[46] Y. Li, J. K. Cooper, W. Liu, C. M. Sutter-Fella, M. Amani, J. W. Beeman, A. Javey, J. W. Ager, Y. Liu, F. M. Toma, I. D. Sharp, *Nature Commun.* **2016**, *7*, 12446.
[47] Q. Tai, P. You, H. Sang, Z. Liu, C. Hu, H. L. W. Chan, F. Yan, *Nature Commun.* **2016**, *7*, 11105.
[48] Y. Zhao, J. Wei, H. Li, Y. Yan, W. Zhou, D. Yu, Q. Zhao, *Nature Commun.* **2016**, *7*, 10228.
[49] P. Cui, D. Wei, J. Ji, D. Song, Y. Li, X. Liu, J. Huang, T. Wang, J. You, M. Li, *Solar RRL* **2017**, *1*, 1600027.
[50] G. E. Eperon, S. D. Stranks, C. Menelaou, M. B. Johnston, L. M. Herz, H. J. Snaith, *Energy Environ. Sci.* **2014**, *7*, 982.
[51] A. Ummadisingu, L. Steier, J.-Y. Seo, T. Matsui, A. Abate, W. Tress, M. Gratzel, *Nature* **2017**, *545*, 208.
[52] L. M. Pazos-Outon, M. Szumilo, R. Lamboll, J. M. Richter, M. Crespo-Quesada, M. Abdi-Jalebi, H. J. Beeson, M. Vrucinic, M. Alsari, H. J. Snaith, B. Ehrler, R. H. Friend, F. Deschler, *Science* **2016**, *351*, 1430.
[53] W. Nie, J.-C. Blancon, A. J. Neukirch, K. Appavoo, H. Tsai, M. Chhowalla, M. A. Alam, M. Y. Sfeir, C. Katan, J. Even, S. Tretiak, J. J. Crochet, G. Gupta, A. D. Mohite, *Nature Commun.* **2016**, *7*, 11574.
[54] S. Chen, X. Wen, S. Huang, F. Huang, Y. Cheng, M. Green, A. Ho-Baillie, *Solar RRL* **2017**, *1*, 1600001.
[55] H. Choi, J. Jeong, H.-B. Kim, S. Kim, B. Walker, G.-H. Kim, J. Y. Kim, *Nano Energy* **2014**, *7*, 80.
[56] J.-W. Lee, D.-H. Kim, H.-S. Kim, S.-W. Seo, S. M. Cho, N.-G. Park, *Adv. Energy Mater.* **2015**, *5*, 1501310.
[57] C. Yi, J. Luo, S. Meloni, A. Boziki, N. Ashari-Astani, C. Graetzel, S. M. Zakeeruddin, U. Roethlisberger, M. Graetzel, *Energy Environ. Sci.* **2016**, *9*, 656.
[58] M. Saliba, T. Matsui, J.-Y. Seo, K. Domanski, J.-P. Correa-Baena, M. K. Nazeeruddin, S. M. Zakeeruddin, W. Tress, A. Abate, A. Hagfeldt, M. Gratzel, *Energy Environ. Sci.* **2016**, *9*.
[59] M. Kulbak, D. Cahen, G. Hodes, *J. Phys. Chem. Lett.* **2015**, *6*, 2452.
[60] M. Kulbak, S. Gupta, N. Kedem, I. Levine, T. Bendikov, G. Hodes, D. Cahen, *J. Phys. Chem. Lett.* **2016**, *7*, 167.
[61] Z. Zhang, Z. Chen, J. Zhang, W. Chen, J. Yang, X. Wen, B. Wang, N. Kobamoto, L. Yuan, J. A. Stride, G. J. Conibeer, R. J. Patterson, S. Huang, *Adv. Energy Mater.* **2017**, *7*, 1601773.
[62] J. Liang, C. Wang, Y. Wang, Z. Xu, Z. Lu, Y. Ma, H. Zhu, Y. Hu, C. Xiao, X. Yi, G. Zhu, H. Lv, L. Ma, T. Chen, Z. Tie, Z. Jin, J. Liu, *J. Am. Chem. Soc.* **2016**, *138*, 15829.
[63] J. Liang, C. Wang, Y. Wang, Z. Xu, Z. Lu, Y. Ma, H. Zhu, Y. Hu, C. Xiao, X. Yi, G. Zhu, H. Lv, L. Ma, T. Chen, Z. Tie, Z. Jin, J. Liu, *Am. Chem. Soc.* **2017**, *139*, 2852.
[64] M. Saliba, T. Matsui, K. Domanski, J.-Y. Seo, A. Ummadisingu, S. M. Zakeeruddin, J.-P. Correa-Baena, W. R. Tress, A. Abate, A. Hagfeldt, M. Gratzel, *Science* **2016**, *354*, 206.
[65] A. Swarnkar, A. R. Marshall, E. M. Sanehira, B. D. Chernomordik, D. T. Moore, J. A. Christians, T. Chakrabarti, J. M. Luther, *Science* **2016**, *354*, 92.
[66] L. Protesescu, S. Yakunin, M. I. Bodnarchuk, F. Krieg, R. Caputo, C. H. Hendon, R. X. Yang, A. Walsh, M. V. Kovalenko, *Nano Lett.* **2015**, *15*, 3692.
[67] J. Song, J. Li, X. Li, L. Xu, Y. Dong, H. Zeng, *Adv. Mater.* **2015**, *27*, 7162.
[68] X. Zhang, B. Xu, J. Zhang, Y. Gao, Y. Zheng, K. Wang, X. W. Sun, *Adv. Funct. Mater.* **2016**, *26*, 4595.
[69] X. Li, Y. Wu, S. Zhang, B. Cai, Y. Gu, J. Song, H. Zeng, *Adv. Funct. Mater.* **2016**, *26*, 2435.
[70] N. Yantara, S. Bhaumik, F. Yan, D. Sabba, H. A. Dewi, N. Mathews, P. P. Boix, H. V. Demir, S. Mhaisalkar, *J. Phys. Chem. Lett.* **2015**, *6*, 4360.
[71] H.-C. Wang, S.-Y. Lin, A.-C. Tang, B. P. Singh, H.-C. Tong, C.-Y. Chen, Y.-C. Lee, T.-L. Tsai, R.-S. Liu, *Angew. Chem. Int. Ed.* **2016**, *55*, 7924.
[72] J. Li, L. Xu, T. Wang, J. Song, J. Chen, J. Xue, Y. Dong, B. Cai, Q. Shan, B. Han, H. Zeng, *Adv. Mater.* **2017**, *29*, 1603885.
[73] C. C. Stoumpos, C. D. Malliakas, J. A. Peters, Z. Liu, M. Sebastian, J. Im, T. C. Chasapis, A. C. Wibowo, D. Y. Chung, A. J. Freeman, B. W. Wessels, M. G. Kanatzidis, *Cryst. Growth Des.* **2013**, *13*, 2722.
[74] R. E. Beal, D. J. Slotcavage, T. Leijtens, A. R. Bowring, R. A. Belisle, W. H. Nguyen, G. F. Burkhard, E. T. Hoke, M. D. McGehee, *J. Phys. Chem. Lett* **2016**, *7*, 746.
[75] Y. Rakita, N. Kedem, S. Gupta, A. Sadhanala, V. Kalchenko, M. L. BOhm, M. Kulbak, R. H. Friend, D. Cahen, G. Hodes, *Cryst. Growth Des* **2016**, *16*, 5717.
[76] D. N. Dirin, I. Cherniukh, S. Yakunin, Y. Shynkarenko, M. V. Kovalenko, *Chem. Mater.* **2016**, *28*, 8470.
[77] I. Chung, B. Lee, J. He, R. P. H. Chang, M. G. Kanatzidis, *M. G., Nature* **2012**, *485*, 486.
[78] R. J. Sutton, G. E. Eperon, L. Miranda, E. S. Parrott, B. A. Kamino, J. B. Patel, M. T. Horantner, M. B. Johnston, A. A. Haghighirad, D. T. Moore, H. J. Snaith, *Adv. Energy Mater.* **2016**, *6*, 1502458.
[79] Q. Ma, S. Huang, X. Wen, M. A. Green, A. W. Y. Ho-Baillie, *Adv. Energy Mater.* **2016**, *6*, 1502202.
[80] H. Chung, S. Il Jung, H. J. Kim, W. Cha, E. Sim, D. Kim, W.-K. Koh, J. Kim, *Angew. Chem. Int. Ed* **2017**, *56*, 4160.
[81] G. R. Yettapu, D. Talukdar, S. Sarkar, A. Swarnkar, A. Nag, P. Ghosh, P. Mandal, *Nano Lett.* **2016**, *16*, 4838.
[82] K. Wu, G. Liang, Q. Shane, Y. Ren, D. Kong, T. Lian, *J. Am. Chem. Soc.* **2015**, *137*, 12792.
[83] Y.-F. Xu, M.-Z. Yang, B.-X. Chen, X.-D. Wang, H.-Y. Chen, D.-B. Kuang, C.-Y. Su, *J. Am. Chem. Soc.* **2017**, *139*, 5660.
[84] J. Lin, L. Gomez, C. de Weerd, Y. Fujiwara, T. Gregorkiewicz, K. Suenaga, *Nano Lett.* **2016**, *16*, 7198.
[85] A. Swarnkar, R. Chulliyil, V. K. Ravi, M. Irfanullah, A. Chowdhury, A. Nag, *Angew. Chem. Int. Ed.* **2015**, *54*, 15424.
[86] Y. Wang, X. Li, X. Zhao, L. Xiao, H. Zeng, H. Sun, *Nano Lett.* **2016**, *16*, 448.
[87] Q. A. Akkerman, V. D'Innocenzo, S. Accornero, A. Scarpellini, A. Petrozza, M. Prato, L. Manna, *J. Am. Chem. Soc.* **2015**, *137*, 10276.
[88] T. L. Doane, K. L. Ryan, L. Pathade, K. J. Cruz, H. Zang, M. Cotlet, M. M. Maye, *ACS Nano* **2016**, *10*, 5864.
[89] X. Chen, H. Hu, Z. Xia, W. Gao, W. Gou, Y. Qu, Y. J. Ma, *Mater. Chem. C* **2017**, *5*, 309.
[90] B. A. Koscher, N. D. Bronstein, J. H. Olshansky, Y. Bekenstein, A. P. Alivisatos, *J. Am. Chem. Soc.* **2016**, *138*, 12065.
[91] G. Nedelcu, L. Protesescu, S. Yakunin, M. I. Bodnarchuk, M. J. Grotevent, M. V. Kovalenko, *Nano Lett.* **2015**, *15*, 5635.
[92] D. Zhang, Y. Yu, Y. Bekenstein, A. B. Wong, A. P. Alivisatos, P. Yang, *J. Am. Chem. Soc.* **2016**, *138*, 13155.
[93] Q. A. Akkerman, S. G. Motti, A. R. S. Kandada, E. Mosconi, V. D'Innocenzo, G. Bertoni, S. Marras, B. A. Kamino, L. Miranda, F. De Angelis, A. Petrozza, M. Prato, L. Manna, *J. Am. Chem. Soc.* **2016**, *138*, 1010.
[94] D. Zhang, S. W. Eaton, Y. Yu, L. Dou, P. Yang, *J. Am. Chem. Soc.* **2015**, *137*, 9230.
[95] J. Shamsi, Z. Dang, P. Bianchini, C. Canale, F. Di Stasio, R. Brescia, M. Prato, L. Manna, *J. Am. Chem. Soc.* **2016**, *138*, 7240.
[96] Y. Bekenstein, B. A. Koscher, S. W. Eaton, P. Yang, A. P. Alivisatos, *J. Am. Chem. Soc.* **2015**, *137*, 16008.

[97] D. Amgar, A. Stern, D. Rotem, D. Porath, L. Etgar, *Nano Lett*. **2017**, *17*, 1007.
[98] S. Seth, A. Samanta, *Sci. Rep*. **2016**, *6*, 37693.
[99] T. Udayabhaskararao, M. Kazes, L. Houben, H. Lin, D. Oron, *Chem. Mater*. **2017**, *29*, 1302.
[100] A. Pan, B. He, X. Fan, Z. Liu, J. J. Urban, A. P. Alivisatos, L. He, Y. Liu, *ACS Nano* **2016**, *10*, 7943.
[101] S. Sun, D. Yuan, Y. Xu, A. Wang, Z. Deng, *ACS Nano* **2016**, *10*, 3648.
[102] H. Wells, *Anorg. Chemie* **1893**, *3*, 195.
[103] C. Moller, *Nature* **1958**, *182*, 1426.
[104] X. Li, F. Cao, D. Yu, J. Chen, Z. Sun, Y. Shen, Y. Zhu, L. Wang, Y. Wei, Y. Wu, H. Zeng, *Small* **2017**, *13*, 1603996.
[105] Q. Le, M. Park, W. Sohn, H. Jang, S. Kim, *Adv. Electron. Mater*. **2017**, *3*, 1600448.
[106] S. Wei, Y. Yang, X. Kang, L. Wang, L. Huang, D. Pan, *Inorg. Chem*. **2017**, *56*, 2596.
[107] G. E. Eperon, G. M. Paterno, R. J. Sutton, A. Zampetti, A. A. Haghighirad, F. Cacialli, H. J. Snaith, *J. Mater. Chem. A* **2015**, *3*, 19688.
[108] P. Luo, W. Xia, S. Zhou, L. Sun, J. Cheng, C. Xu, Y. Lu, *J. Phys. Chem. Lett*. **2016**, *7*, 3603.
[109] Y. G. Kim, T.-Y. Kim, J. H. Oh, K. S. Choi, Y.-J. Kim, S. Y. Kim, *Phys. Chem. Chem. Phys*. **2017**, *19*, 6257.
[110] C. F. J. Lau, X. Deng, Q. Ma, J. Zheng, J. S. Yun, M. A. Green, S. Huang, A. W. Y. Ho-Baillie, *ACS Energy Lett*. **2016**, *1*, 573.
[111] J. Scott Niezgoda, B. Foley, A. Chen, J. Choi, *ACS Energy Lett*. **2017**, *2*, 1043.
[112] J. K. Nam, S. U. Chai, W. Cha, Y. J. Choi, W. Kim, M. S. Jung, J. Kwon, D. Kim, J. H. Park, *Nano Lett*. **2017**, *17*.
[113] M. H. Kumar, S. Dharani, W. L. Leong, P. P. Boix, R. R. Prabhakar, T. Baikie, C. Shi, H. Ding, R. Ramesh, M. Asta, M. Graetzel, S. G. Mhaisalkar, N. Mathews, *Adv. Mater*. **2014**, *26*, 7122.
[114] T.-B. Song, T. Yokoyama, C. C. Stoumpos, J. Logsdon, D. H. Cao, M. R. Wasielewski, S. Aramaki, M. G. Kanatzidis, *J. Am. Chem. Soc*. **2017**, *139*, 836.
[115] N. Wang, Y. Zhou, M.-G. Ju, H. F. Garces, T. Ding, S. Pang, X. C. Zeng, N. P. Padture, X. W. Sun, *Adv. Energy Mater*. **2016**, *6*, 1601130.
[116] S. Gupta, T. Bendikov, G. Hodes, D. Cahen, *ACS Energy Lett*. **2016**, *1*, 1028.
[117] B. Wu, Y. Zhou, G. Xing, Q. Xu, H. F. Garces, A. Solanki, T. W. Goh, N. P. Padture, T. C. Sum, *Adv. Funct. Mater*. **2017**, *27*, 1604818.
[118] X. Li, D. Yu, F. Cao, Y. Gu, Y. Wei, Y. Wu, J. Song, H. Zeng, *Adv. Funct. Mater*. **2016**, *26*, 5903.
[119] J.-H. Cha, J. H. Han, W. Yin, C. Park, Y. Park, T. K. Ahn, J. H. Cho, D.-Y. Jung, *J. Phys. Chem. Lett*. **2017**, *8*, 565.
[120] L. Zhou, K. Yu, F. Yang, J. Zheng, Y. Zuo, C. Li, B. Cheng, Q. Wang, *Dalton Trans*. **2017**, *46*, 1766.
[121] L. Lv, Y. Xu, H. Fang, W. Luo, F. Xu, L. Liu, B. Wang, X. Zhang, D. Yang, W. Hu, A. Dong, *Nanoscale* **2016**, *8*, 13589.
[122] J. Song, L. Xu, J. Li, J. Xue, Y. Dong, X. Li, H. Zeng, *Adv. Mater*. **2016**, *28*, 4861.
[123] X. Li, D. Yu, J. Chen, Y. Wang, F. Cao, Y. Wei, Y. Wu, L. Wang, Y. Zhu, Z. Sun, J. Ji, Y. Shen, H. Sun, H. Zeng, *ACS Nano* **2017**, *11*.
[124] D. Zhang, Y. Yang, Y. Bekenstein, Y. Yu, N. A. Gibson, A. B. Wong, S. W. Eaton, N. Kornienko, Q. Kong, M. Lai, A. P. Alivisatos, S. R. Leone, P. Yang, *J. Am. Chem. Soc*. **2016**, *138*, 7236.
[125] P. Ramasamy, D.-H. Lim, B. Kim, S.-H. Lee, M.-S. Lee, J.-S. Lee, *Chem. Commun*. **2016**, *52*.
[126] X. Tong, W. Kong, Y. Wang, J. Zhu, L. Luo, Z. Wang, *ACS Appl. Mater. Interfaces* **2017**, *9*, 18977.
[127] H. Huang, H. Lin, S. V. Kershaw, A. S. Susha, W. C. H. Choy, A. L. Rogach, *J. Phys. Chem. Lett*. **2016**, *7*, 4398.
[128] G. Li, F. W. R. Rivarola, N. J. L. K. Davis, S. Bai, T. C. Jellicoe, F. de la Pena, S. Hou, C. Ducati, F. Gao, R. H. Friend, N. C. Greenham, Z.-K. Tan, *Adv. Mater*. **2016**, *28*, 3528.
[129] Y. H. Song, J. S. Yoo, B. K. Kang, S. H. Choi, E. K. Ji, H. S. Jung, D. H. Yoon, *Nanoscale* **2016**, *8*, 19523.
[130] C. C. Lin, A. Meijerink, R.-S. Liu, *J. Phys. Chem. Lett*. **2016**, *7*, 495.
[131] Z. Wei, A. Perumal, R. Su, S. Sushant, J. Xing, Q. Zhang, S. T. Tan, H. V. Demir, Q. Xiong, *Nanoscale* **2016**, *8*, 18021.
[132] Q. Jiang, M. Chen, J. Li, M. Wang, X. Zeng, T. Besara, J. Lu, Y. Xin, X. Shan, B. Pan, C. Wang, S. Lin, T. Siegrist, Q. Xiao, Z. Yu, *ACS Nano* **2017**, *11*, 1073.
[133] L. Quyet Van, M. Park, W. Sohn, H. W. Jang, S. Y. Kim, *Adv. Electron. Mater*. **2017**, *3*, 1600448.
[134] G. Li, H. Wang, T. Zhang, L. Mi, Y. Zhang, Z. Zhang, W. Zhang, Y. Jiang, *Adv. Funct. Mater*. **2016**, *26*, 8478.
[135] C. Guhrenz, A. Benad, C. Ziegler, D. Haubold, N. Gaponik, A. Eychmuller, *Chem. Mater*. **2016**, *28*, 9033.
[136] M. Meyns, M. Peralvarez, A. Heuer-Jungemann, W. Hertog, M. Ibanez, R. Nafria, A. Genc, J. Arbiol, M. V. Kovalenko, J. Carreras, A. Cabot, A. G. Kanaras, *ACS Appl. Mater. Interfaces* **2016**, *8*, 19579.
[137] X. Zhang, H. Lin, H. Huang, C. Reckmeier, Y. Zhang, W. C. H. Choy, A. L. Rogach, *Nano Lett*. **2016**, *16*, 1415.
[138] Z. Shi, Y. Li, Y. Zhang, Y. Chen, X. Li, D. Wu, T. Xu, C. Shan, G. Du, *Nano Lett*. **2017**, *17*, 313.
[139] J. Pan, L. N. Quan, Y. Zhao, W. Peng, B. Murali, S. P. Sarmah, M. Yuan, L. Sinatra, N. M. Alyami, J. Liu, E. Yassitepe, Z. Yang, O. Voznyy, R. Comin, M. N. Hedhili, O. F. Mohammed, Z. H. Lu, D. H. Kim, E. H. Sargent, O. M. Bakr, *Adv. Mater*. **2016**, *28*, 8718.
[140] Y. Ling, Y. Tian, X. Wang, J. C. Wang, J. M. Knox, F. Perez-Orive, Y. Du, L. Tan, K. Hanson, B. Ma, H. Gao, *Adv. Mater*. **2016**, *28*, 8983.
[141] W.-L. Hong, Y.-C. Huang, C.-Y. Chang, Z.-C. Zhang, H.-R. Tsai, N.-Y. Chang, Y.-C. Chao, *Adv. Mater*. **2016**, *28*, 8029.